TITLE: Interneuron Control of *C. elegans* Developmental Decision-making

AUTHORS: Cynthia M. Chai[1], Mahdi Torkashvand[2], Maedeh Seyedolmohadesin[2], Heenam Park[1], Vivek Venkatachalam[2], Paul W. Sternberg[1†]

AFFILIATIONS:

[1]Division of Biology and Biological Engineering, California Institute of Technology, Pasadena 91125, California, USA

[2]Department of Physics, Northeastern University, Boston 02115, Massachusetts, USA

[†]**CORRESPONDING AUTHOR:**

Paul W. Sternberg (pws@caltech.edu)

SUMMARY

Animals integrate external stimuli to shape their physiological responses throughout development. In adverse environments, *Caenorhabditis elegans* larvae can enter a stress-resistant diapause state with arrested metabolism and reproductive physiology. Amphid sensory neurons feed into both rapid chemotactic and short-term foraging mode decisions, mediated by amphid and pre-motor interneurons, as well as the long-term diapause decision. We identify amphid interneurons that integrate pheromone cues and propagate this information via a neuropeptidergic pathways to influence larval developmental fate, bypassing the pre-motor system. AIA interneuron-derived FLP-2 neuropeptide signaling promotes reproductive growth and AIA activity is suppressed by pheromone. FLP-2 acts antagonistically to the insulin-like INS-1. FLP-2's growth promoting effects are inhibited by upstream metabotropic glutamatergic signaling and mediated by the broadly-expressed neuropeptide receptor NPR-30. Conversely, the AIB interneurons and their neuropeptide receptor NPR-9/GALR2 promote diapause entry. These neuropeptidergic outputs allow reuse of parts of a sensory system for a decision with a distinct timescale.

KEYWORDS

Developmental plasticity, interneurons, neuropeptides, G-protein coupled receptor, pheromone, circuits, metabotropic glutamate receptor, inter-tissue signaling, physiology, metabolism

INTRODUCTION

Natural environments are highly dynamic and this complexity challenges animals to accurately integrate external cues to shape their responses. Phenotypic plasticity is the ability of a single genotype to produce more than one phenotype depending on the external environment experienced. Adaptive developmental plasticity enables organisms to remodel their physiology, morphology, and behavior to better suit the predicted future environment and ultimately enhance their ecological success (Kelly et al., 2012). Developmental plasticity often results in long-lasting changes such as switches in developmental trajectories that irreversibly alter the adult phenotype or, in some cases, induce reversible developmental arrest. This adaptive strategy is employed throughout the animal kingdom by nematodes (Bento et al., 2010; Cassada and Russell, 1975), arthropods (Brakefield et al., 1998; Laforsch et al., 2006; Moczek and Emlen, 2000), fish (Podrabsky and Hand, 1999), reptiles (Janzen and Paukstis, 1991), and amphibians (Michimae and Wakahara, 2001; Pfennig, 1992). Although it is known that sensory cues usually trigger the developmental switch and that downstream inter-tissue signaling pathways enact the alternative developmental phenotype, the integrative neural mechanisms that transduce external inputs into effector pathways are less clear (Beldade et al., 2011; Nijhout, 2003). Developmental fate choice requires sensory evidence accumulation to surpass an innately-defined threshold, signaling the appropriateness of selecting a particular trajectory over the other. Understanding how an animal generates a neural representation of current and forecasted environmental conditions and converts these circuit computations into a predictive adaptive physiological response might provide fundamental insights into the molecular and cellular basis of decision-making over developmentally-relevant timescales.

Here, we leverage the well-defined genetics and nervous system of the microscopic roundworm *Caenorhabditis elegans* to dissect the sensory integration pathways controlling larval developmental plasticity. Under adverse environmental conditions, *C. elegans* L1 stage larvae can enter an alternate stress-resistant diapause state during which metabolism and reproductive physiology are arrested(Golden and Riddle, 1984). The transition into diapause is accompanied by adaptations that enable the larva to endure and survive deleterious conditions. Dauer larvae possess thickened cuticles, enlarged intestinal lipid droplets, arrested gonad development, and are radially constricted compared to their reproductive L3 stage counterparts (Cassada and Russell, 1975). They also exhibit dauer stage-specific behaviors such as nictation, carbon dioxide attraction, and cessation of pharyngeal pumping (Cassada and Russell, 1975; Hallem et al., 2011; Lee et al., 2011). Once in the dauer stage, larvae can survive for several months without food and can revert to the reproductive trajectory at any point during this period should a favorable shift in external conditions occur (Cassada and Russell, 1975; Klass and Hirsh, 1976). The *C. elegans* larval decision to enter diapause is informed by multimodal sensory cues

68 (Figure 1A). Coincident detection of high pheromone concentrations, high temperatures, and low food
69 availability by the larval sensory apparatus triggers diapause entry (Golden and Riddle, 1982; 1984). *C.*
70 *elegans* constitutively secretes a mixture nematode-specific glycosides called ascarosides that
71 comprise dauer larvae-inducing pheromone, which serves as a measure of local conspecific
72 competition for limited resources (Butcher et al., 2008; Jeong et al., 2005; Pungaliya et al., 2009).
73 These small-molecule ascarosides bind to seven transmembrane domain receptors located in
74 chemosensory neuron cilia to trigger intracellular signaling cascades that alter neuronal activity (Kim et
75 al., 2009; McGrath et al., 2011).
76 The majority of previous literature on the neural control of *C. elegans* diapause entry has
77 focused on the contributions of sensory neurons. Systematic laser and genetic ablations of sensory
78 neuron classes have revealed that six of the eleven amphid chemosensory neuron classes mediate
79 diapause entry (Bargmann and Horvitz, 1991; Kim *et al.*, 2009; Schackwitz et al., 1996). In *C. elegans*,
80 sensory neurons are also the main sources of neuroendocrine ligands like DAF-7/TGF-ß (ASI neurons)
81 and neuromodulators like serotonin (ADF neurons) that promote reproductive growth by acting on
82 multiple tissues (Schackwitz *et al.*, 1996; Sze et al., 2000). It is thus plausible that sensory layer circuits
83 account for all integrative computations of multimodal stimuli, which then bypasses interneuron
84 processing by directly executing secretory signaling pathways to influence developmental fate. In
85 contrast, *C. elegans* neurobehavioral studies generally involve a hierarchical organization of information
86 flow from the sensory layer to interneurons and finally to effector motor neurons (Figure 1B; Faumont et
87 al., 2012). The first layer amphid interneurons AIA, AIB, AIY, and AIZ are so termed because they
88 receive extensive synaptic inputs from sensory neurons residing within the amphid organ in the head
89 (White et al., 1986). They then relay this information to the second layer amphid interneurons RIA, RIB,
90 and RIM, which are presynaptic to command-like interneurons (White et al., 1986).
91 In this study, we combine classical genetics methods with chemogenetics, calcium imaging, and
92 precision genome editing to examine whether a similar circuit hierarchy is involved in controlling *C.*
93 *elegans* developmental plasticity (Figure 1B). To model the stressful dauer-inducing conditions
94 encountered by *C. elegans* in the wild, we incubated developing larvae at elevated temperatures while
95 continuously exposing them to crude pheromone extract and a low-quality, limited food source (Lee et
96 al., 2017). The number of larvae that developed into dauers and non-dauer reproductive adults were
97 scored and used to calculate a dauer formation index value for each assay plate (see Methods). A
98 more positive index value indicates a greater tendency to form dauers while a more negative index
99 value denotes a preference for entering the reproductive developmental trajectory. We find that the AIA
100 interneurons contribute to developmental fate choice by integrating conspecific cues and propagating
101 this information via neuropeptide signaling, in particular by the RF-amide neuropeptide encoded by *flp-*

102 *2*. AIA-derived FLP-2 signaling promotes reproductive growth and is inhibited by upstream
103 glutamatergic signaling via the metabotropic glutamate receptor MGL-1. FLP-2 signaling, which we
104 show antagonizes insulin-like INS-1 signaling, is mediated by the downstream neuropeptide G-protein
105 coupled receptor NPR-30, expressed in neurons and the intestine. Furthermore, AIA's major
106 postsynaptic partners, the NPR-9/GALR2-expressing AIB interneurons, promotes diapause entry
107 suggesting an antagonistic relationship between both interneuron classes in this decision-making
108 paradigm. Our findings reveal a role for the first layer amphid interneurons in coupling sensory stimuli
109 detection to downstream neuropeptide pathways mediating inter-tissue signaling during developmental
110 decision-making.
111

112 **RESULTS**

113 **AIA inhibition recapitulates the increased dauer formation phenotype of a *flp-2* mutant**

114 To investigate if AIA activity affects larval developmental trajectory, we pharmacologically
115 silenced AIA by expressing the *Drosophila* histamine-gated chloride channel HisCl1 (Pokala et al.,
116 2014). *C. elegans* neither synthesizes nor uses histamine as an endogenous neurotransmitter (Chase
117 and Koelle, 2007). We constitutively silenced AIA by growing AIA::*HisCl1* animals on plates containing
118 histamine and compared dauer formation with animals of the same genotype grown on control plates
119 without histamine. We found that a significantly higher proportion of AIA-silenced animals entered
120 diapause compared to the negative control, indicating that AIA promotes entry into the reproductive
121 growth trajectory (Figure 1C).

122 As AIA inhibition increases dauer formation, AIA likely promotes reproductive growth. Given the
123 relatively long timescale of the diapause entry decision, we considered the role of modulatory
124 neuropeptides. The *flp* gene family encodes FMRFamide-like neuropeptides, some of which have been
125 implicated in regulating pheromone-induced dauer formation (Lee *et al.*, 2017). Similar to chemogenetic
126 silencing of AIA, *flp-2*(*ok3351*) mutants form more dauers compared to wild-type controls (Figure 1D;
127 Lee *et al.*, 2017). The *ok3351* allele harbors a deletion that removes the first exon of both predicted *flp-*
128 *2* transcripts and is thus likely to be a null mutation. *flp-2* expression has been reported in the AIA, RID,
129 PVW, I5 and MC neurons (Kim and Li, 2004). A transcriptional reporter containing a truncated 2 kb
130 fragment of upstream regulatory sequence 5' to the *flp-2* start codon fused to GFP was expressed
131 strongly and consistently in a single pair of neurons in the head during the L1 stage (Figure 1E). We
132 identified this pair of neurons as the AIA interneurons based on GFP expression colocalization with a
133 nuclear-localized AIA-specific mCherry marker (Figure 1E; Shinkai et al., 2011).
134

135 **AIA-derived FLP-2 promotes larval entry into the reproductive growth trajectory**

136 To determine if FLP-2 mediates AIA's reproductive growth-promoting role, we expressed *flp-2*
137 cDNA specifically in AIA where it was sufficient to rescue the *flp-2(-)* dauer formation phenotype (Figure
138 2A). Some non-neuronal GFP expression was also visible in the intestine of the *flp-2* transcriptional
139 GFP reporter but intestine-specific *flp-2* cDNA expression did not affect *flp-2(-)* mutant dauer formation
140 (Figure S1). Since loss of FLP-2 signaling in the *flp-2(-)* mutant leads to increased dauer formation, we
141 wondered if an excess of the neuropeptide would have the opposite effect on larval development.
142 Indeed, AIA-specific overexpression of *flp-2* cDNA resulted in reduced dauer formation compared to
143 control animals (Figure 2C).
144 To confirm that FLP-2 peptides are secreted by AIA, we fused mCherry to the C-terminus of
145 FLP-2 precursors expressed in AIA. We detected both diffuse and vesicular mCherry expression in
146 AIA's soma, which was visualized by soluble GFP (Figure 2D). In *C. elegans,* secreted proteins are
147 released into the pseudocoelom and endocytosed by the coelomocyte scavenger cells (Fares and
148 Greenwald, 2001). The six coelomocyte scavenger cells are located in three pairs along the animal's
149 body. During the L1 stage, we observed strong mCherry signal within GFP-expressing coelomocyte
150 cells indicating FLP-2 peptide release and uptake (Figure 2E). Taken together, these results indicate
151 that FLP-2 is an AIA-secreted signal that promotes reproductive development.
152
153 **Pheromone activates ASK and ADL sensory neurons but inhibits downstream AIA interneurons**
154 The AIA interneurons make several chemical and electrical synaptic connections with the
155 amphid chemosensory neuron classes including ASK and ADL, which mediate adult responses to
156 certain ascarosides (Figure 3A; Jang et al., 2012; Macosko et al., 2009; White *et al.*, 1986). Laser
157 microbeam ablation and mutant analysis of ASK and ADL indicate that these sensory neurons promote
158 dauer formation (Bargmann and Horvitz, 1991; Kim et al., 2009; Schackwitz et al., 1996). To examine
159 the relationship between sensory neuron activity and dauer formation, we silenced ASK and ADL by
160 selective expression of *Drosophila* HisCl1. Silencing of either neuron class reduced dauer formation
161 suggesting that ASK and ADL activity promotes diapause entry (Figure 3B,D). We note that the effect
162 size of ADL silencing is smaller compared to ASK silencing suggesting a subtler physiological
163 contribution by ADL during dauer formation. In adult animals, ASK intracellular calcium levels are
164 decreased by exposure to synthetic ascaroside cocktails that mediate adult aggregation (Macosko et
165 al., 2009). However, the crude pheromone extract used in this study is a mixture of ascaroside
166 components in naturally-occurring proportions whose synergistic effects might elicit different responses.
167 We sought to determine if and how crude pheromone extract modulates ASK and ADL responses by
168 delivering a time-locked pheromone stimulus to restrained L4 stage animals expressing the genetically-
169 encoded calcium sensor GCaMP6s in both neuron classes (Chen et al., 2013). Pheromone delivery

170 was accompanied by a fast, robust increase in intracellular calcium levels in ASK and ADL indicating
171 that both sensory neuron classes detect and are activated by crude pheromone (Figure 3C,E). In
172 addition, both paired partners of each sensory neuron class displayed symmetric responses to
173 pheromone delivery (Figure 3C,E).

174 AIA is depolarized when animals are presented with synthetic ascaroside mixtures (Macosko et
175 al., 2009). To probe if AIA responds similarly to crude pheromone extract, we delivered pheromone to
176 physically-restrained L4 animals expressing GCaMP6s in AIA only. We first recorded calcium influx
177 changes in AIA's soma and could not detect any significant changes in AIA activity during pheromone
178 delivery (Figure S2). As *C. elegans* interneurons exhibit compartmentalized calcium dynamics, we next
179 measured GCaMP fluorescence changes in the AIA processes within the nerve ring where synaptic
180 connections are densely concentrated (Hendricks et al., 2012). In our microfluidics setup, AIA is
181 frequently quiescent with only 20% of all animals assayed displaying any process activity during
182 experiments. In this fraction of animals, pheromone delivery consistently suppressed spontaneous AIA
183 process activity and removal of the pheromone stimulus was followed by a post-inhibitory activity
184 rebound that was greater in amplitude compared to before pheromone delivery (Figure 3F). Thus, AIA
185 activity is inhibited by crude pheromone extract. Furthermore, the opposite responses to pheromone of
186 ASK and ADL compared to AIA implies that ASK and ADL make inhibitory connections to downstream
187 AIA interneurons.

188 The AWA olfactory sensory neurons sense and mediate *C. elegans* chemoattraction to the
189 odorant diacetyl, and are gap-junctioned to AIA (Figure 3A; Bargmann et al., 1993; White et al., 1986).
190 Diacetyl is a bacterial metabolite and might serve as a growth-promoting food signal to the
191 bacteriovorous *C. elegans*. An AND-gate logic model of AIA integrative function has previously been
192 proposed where coincident inhibition of glutamatergic chemosensory neurons including ASK and
193 activation of AWA by diacetyl leads to robust AIA activation in adult animals (Dobosiewicz et al., 2019).
194 We wondered if exposure to diacetyl concentrations that mediate adult behavioral responses might bias
195 larval development towards the reproductive trajectory under our pheromone dauer-inducing assay
196 conditions. However, we found that diacetyl exposure throughout the assay duration did not affect
197 dauer formation compared to control assays with ethanol diluent only (Figure 3G). Behavioral
198 responses to diacetyl differ between larval and adult *C. elegans*, with larvae displaying a weaker
199 response (Fujiwara et al., 2016). Thus, stage-specific differences in sensory processing might account
200 for the lack of developmental effects of diacetyl exposure in our dauer formation assays. Furthermore,
201 the longer timescale of diacetyl exposure during dauer formation assays might also affect sensory
202 neuron-to-AIA circuit dynamics differently compared to acute diacetyl presentation in a microfluidics
203 device (Dobosiewicz et al., 2019).

204

205 **FLP-2 signaling is inhibited by upstream glutamatergic transmission via the metabotropic**
206 **glutamate receptor MGL-1**

207 Although glutamate is the major excitatory neurotransmitter in the vertebrate central nervous
208 system, glutamate can also have inhibitory effects depending on the type of glutamate receptors
209 present in the postsynaptic membrane. ASK and ADL are glutamatergic sensory neurons (Serrano-Saiz
210 et al., 2013). AIA expresses both the fast ionotropic glutamate-gated chloride channel GLC-3 and the
211 slow G-protein coupled metabotropic glutamate receptor MGL-1 (Dillon et al., 2006; Greer et al., 2008;
212 Horoszok et al., 2001; Taylor et al., 2021). Thus, it is likely that glutamatergic transmission from
213 upstream ASK and ADL sensory neurons affects AIA-mediated FLP-2 signaling during developmental
214 decision-making.

215 To test this hypothesis, we first determined if *glc-3(-)* mutants had a dauer formation phenotype.
216 Interestingly, *glc-3(-)* mutants exhibited a wider spectrum of developmental phenotypes compared to
217 the binary reproductive adult or arrested dauer phenotypic outcomes observed for other strains in this
218 study. Under pheromone dauer-inducing conditions, *glc-3(-)* mutants also produce a third
219 developmentally-arrested partial dauer phenotype that exhibits lighter-colored bodies and is not as
220 radially-constricted as full dauers (Vowels and Thomas, 1992). *glc-3(-)* partial dauers also display
221 pharyngeal pumping and active locomotory behavior. The intermediate partial dauer phenotype arises
222 from either incomplete tissue remodeling during diapause entry or an inability to maintain complete
223 tissue remodeling once in the dauer stage. When considering both partial dauers and dauers as having
224 entered diapause, *glc-3(-)* mutants enter diapause at levels comparable to control animals (Figure 4A).
225 If partial dauers are considered "non-dauers" that do not meet the criteria for dauer formation, then *glc-*
226 *3(-)* mutants exhibit a reduced dauer formation phenotype (Figure 4B). *flp-2(-)*; *glc-3(-)* double mutants
227 had an additive dauer formation phenotype significantly different from both the *flp-2(-)* and *glc-3(-)*
228 single mutant controls (Figure 4B). Moreover, *flp-2(-)*; *glc-3(-)* double mutants form partial dauers at a
229 level comparable to *glc-3(-)* single mutants. Taken together, these results argue against a role for
230 inhibitory glutamatergic transmission via GLC-3 in regulating FLP-2 signaling during dauer formation
231 (Figure 4B).

232 In contrast, *mgl-1(-)* mutants do not form partial dauers under pheromone dauer-inducing
233 conditions. We found that fewer *mgl-1(-)* mutants developed into dauers compared to control animals
234 suggesting that glutamatergic transmission via MGL-1 promotes pheromone-induced dauer formation
235 (Figure 4C, Figure S3). MGL-1 shares sequence similarity with the mammalian group II inhibitory
236 metabotropic glutamate receptors, suggesting that ASK and ADL glutamatergic transmission might
237 suppress AIA and FLP-2 signaling (Dillon *et al.*, 2006). If FLP-2 signaling is downstream of MGL-1-

238 mediated glutamatergic transmission, we would expect the *flp-2(-)* mutant's increase in dauer formation
239 to mask the *mgl-1(-)* mutant's reduction in dauer formation phenotype in the double mutant, displaying
240 epistasis. As *mgl-1* and *flp-2* genes are on the same chromosome, we generated a *flp-2(-)*; *mgl-1(-)*
241 double mutant by CRISPR mutagenesis of the *mgl-1* locus in a *flp-2(-)* mutant background (see
242 Methods). The *flp-2(-)*; *mgl-1(-)* double mutant phenocopied the *flp-2(-)* single mutant's increased dauer
243 formation phenotype indicating that *flp-2* is in the same genetic pathway as *mgl-1* and acts downstream
244 (Figure 4C). Our results suggest that FLP-2 signaling is inhibited by glutamatergic transmission via the
245 metabotropic glutamate receptor MGL-1.
246
247 **The broadly-expressed neuropeptide receptor NPR-30 is downstream of FLP-2 signaling**
248 We next focused on identifying downstream elements of the AIA-mediated developmental
249 decision-making circuit. *In vitro* studies indicate that peptides cleaved from the FLP-2 precursor protein
250 bind to the G-protein coupled neuropeptide receptor FRPR-18 in a heterologous mammalian cell
251 expression system (Larsen et al., 2013). However, *frpr-18(-)* mutants had a decreased dauer formation
252 phenotype (Figure 5A). Furthermore, *flp-2(-)*; *frpr-18(-)* double mutants exhibit an additive phenotype
253 that is significantly different from both the *flp-2(-)* and *frpr-18(-)* single mutant controls (Figure 5A).
254 These results indicate that *flp-2* and *frpr-18* are not in the same genetic pathway in the context of dauer
255 formation. We continued our search for potential downstream receptor mediators of FLP-2 signaling by
256 testing neuropeptide G-protein coupled receptor mutants that have an increased dauer formation
257 phenotype for their ability to completely suppress the *flp-2* overexpression reduced dauer formation
258 phenotype; this screen identified *npr-30* (Figure 5B). Thus, *npr-30* is downstream of *flp-2* in the same
259 pathway mediating the diapause entry decision.
260 To determine where *npr-30* is expressed, we generated a *npr-30* translational reporter
261 containing an 8.5 kb *npr-30* genomic fragment linked to GFP by an SL2-spliced intercistronic region.
262 During the L1 stage, GFP was broadly expressed in the nervous system as well as in the intestine
263 (Figure 5C). In the nervous system, we observed expression in sensory neurons, interneurons, and
264 motor neurons, suggesting that FLP-2 signaling exerts its global modulatory effects via NPR-30 (Figure
265 5D). Besides acting on other targets, FLP-2 might also mediate an AIA autoregulatory positive
266 feedback loop to drive and sustain commitment to reproductive growth under favorable conditions.
267 However, our *npr-30* translational GFP reporter did not colocalize with an AIA-specific mCherry marker
268 in L1 larvae, suggesting this motif is unlikely (Figure 5E).
269
270 **Insulin-like growth factor INS-1 and FLP-2 have antagonistic roles in developmental decision-**
271 **making**

272 The insulin signaling pathway is an evolutionarily-conserved regulator of energy homeostasis
273 and metabolism. In mammals, insulin signaling promotes lipid storage and inhibits the breakdown of fat
274 (Huang et al., 2020). In *C. elegans*, the larval transition into diapause entails increased lipid storage
275 and decreased fat metabolism to facilitate long-term survival under resource-scarce conditions (Ashrafi,
276 2007). In addition to *flp-2*, AIA co-expresses the insulin-related growth factor-encoding *ins-1* (Kodama
277 et al., 2006). In adult animals, AIA-specific INS-1 release mediates normal turning behavior during
278 odor-evoked local search (Chalasani et al., 2010). Therefore, we decided to investigate if AIA-derived
279 INS-1 might play a role in dauer formation. Under pheromone dauer-inducing conditions, *ins-1(-)*
280 mutants exhibited a decreased dauer formation phenotype indicating that INS-1 signaling promotes
281 diapause entry (Figure 6A). Furthermore, the *flp-2(-)*; *ins-1(-)* double mutant displayed an additive
282 phenotype that was significantly different from both the *flp-2(-)* and *ins-1(-)* single mutant phenotypes,
283 suggesting that these neuropeptides act in independent genetic pathways (Figure 6A). To determine if
284 AIA-derived INS-1 promotes dauer entry, we expressed *ins-1* cDNA in an AIA-specific manner in an
285 *ins-1(-)* mutant background and found that it did not affect the *ins-1(-)* mutant's dauer formation
286 phenotype (Figure 6B). As *ins-1* is expressed in many other neuron classes besides AIA, we propose
287 that INS-1 secretion by other neuron classes antagonizes AIA-derived FLP-2 signaling during
288 pheromone-induced dauer formation (Figure 6C; Kodama *et al.*, 2006).
289
290 **AIB interneurons and their neuropeptide receptor NPR-9/GALR2 promote diapause entry**
291 The AIB interneurons are AIA's main postsynaptic partners and the strong unidirectional
292 synaptic connection from AIA to AIB is likely to be inhibitory based on their opposite functions in
293 behavioral studies (Wakabayashi et al., 2004). Furthermore, AIA is cholinergic and AIB expresses the
294 ACC-1 acetylcholine-gated chloride channel (Pereira et al., 2015; Putrenko et al., 2005; Taylor et al.,
295 2021). However, AIB also expresses excitatory glutamate receptors and receives synaptic inputs from
296 glutamatergic sensory neurons including the pheromone-sensing ADL (Brockie et al., 2001; Serrano-
297 Saiz et al., 2013; White et al., 1986). This observation suggests that excitatory glutamatergic and
298 inhibitory cholinergic neurotransmission from the sensory layer and other pre-motor interneurons,
299 respectively, might compete to shape AIB responses under different environmental conditions.
300 Pharmacological silencing of AIB reduced dauer formation suggesting that the AIA and AIB first
301 layer interneurons have antagonistic effects on larval developmental choice (Figure 7A). *npr-9* encodes
302 a neuropeptide G-protein coupled receptor that is homologous to human galanin receptor 2 (GALR2)
303 and is expressed in the AIB neurons where it mediates adult foraging behavior (Bendena et al., 2008).
304 *npr-9(-)* mutants assayed for pheromone-induced dauer formation recapitulated the AIB-silenced
305 decreased dauer formation phenotype suggesting that AIB's diapause entry-promoting role involves

306 NPR-9 signaling (Figure 7B). We used a genetic epistasis test to determine whether FLP-2 and NPR-9
307 mediate related or independent signaling pathways. As *npr-9* and *flp-2* are also on the same
308 chromosome, we used a similar CRISPR-based strategy as with the *flp-2(-)*; *mgl-1(-)* strain discussed
309 above to generate a *flp-2(-)*; *npr-9(-)* double mutant. The *flp-2(-)*; *npr-9(-)* double mutant phenocopied
310 the *flp-2(-)* single mutant's increased dauer formation phenotype indicating that *flp-2* is downstream of
311 *npr-9* in the same genetic pathway that influences developmental fate (Figure 7B). The decreased
312 dauer formation phenotype of AIB-silenced animals suggests that AIB is activated by adverse
313 environmental cues that promote dauer formation. However, neither AIB's process nor soma exhibited
314 any activity changes in response to acute pheromone delivery in a microfluidics device (Figure 7C,
315 Figure S4). The absence of any AIB response to pheromone presentation alone suggests that AIB
316 activity might be gated by additional sensory inputs that could interact with the pheromone stimulus. As
317 L4 stage animals were used for calcium imaging experiments, it is also possible that stage-specific
318 synaptic connectivity differences might underlie the observed discrepancies between dauer formation
319 assay results and functional imaging data.
320

321 **DISCUSSION**

322 Here, we show that a pair of interneurons controls the switch between different larval
323 developmental trajectories depending on prevailing environmental conditions. Under favorable
324 conditions, AIA is active and secretes FLP-2 neuropeptides, which promotes reproductive growth
325 (Figure 8A). FLP-2 signaling is mediated by the neuropeptide receptor NPR-30 which is broadly
326 expressed in neurons and the intestine (Figure 8A). As conspecific population density and competition
327 for limited resources increases, the concentration of secreted pheromone in the local area also
328 increases. These pheromone cues activate the ASK and ADL sensory neurons, which suppress
329 downstream AIA interneuron activity (Figure 8B). FLP-2 signaling is inhibited by upstream
330 glutamatergic transmission mediated by the metabotropic glutamate receptor MGL-1 resulting in more
331 larvae choosing to enter diapause (Figure 8B). Thus, we have discovered how salient sensory cues are
332 transduced by an integrative interneuron into neuropeptidergic signals that shape larval developmental
333 decision-making. We further expand this decision-making circuit by functionally implicating the AIB
334 interneurons, AIA's main postsynaptic partners, and their NPR-9/GALR2 neuropeptide receptor in
335 promoting diapause entry (Figure 8C).

336 Diapause entry can be maladaptive if an incorrect assessment of environmental conditions is
337 made since dauer larvae can take up to 20 hours to fully re-enter the trajectory leading to reproductive
338 adulthood (Cassada and Russell, 1975). The metabolic costs of physiological remodeling coupled with
339 the delay in nutritional intake (dauers are non-feeding) can negatively impact future reproductive

340 success. Thus, we would expect such an important calculation to be under the control of complex,
341 distributed regulatory networks as opposed to relying on a more efficient sparse-coding scheme that is
342 less robust when challenged with noisy inputs from nature. There are likely to be more neuron classes
343 involved in this circuit, especially other interneurons that lie at the confluence of multiple upstream
344 sensory modalities and have neuromodulatory capabilities. A key motivation behind this study was to
345 determine if information flow during developmental decision-making followed the same generalized
346 hierarchical structure as behavior. Based on our findings, the interneuron layer does contribute to the
347 diapause entry decision in an integrative capacity; it would be interesting to see whether interneuron-
348 derived signals eventually feed back to the sensory layer, which then executes terminal effector
349 pathways that 'locks in' larval fate.

350 The results of our microfluidics experiments show that acute inhibition of AIA by pheromone is
351 followed by a sharp increase in calcium influx immediately after pheromone delivery is terminated. This
352 observed post-inhibitory increase in AIA activity appears to contradict our functional dauer formation
353 assay results which suggest that dauer-inducing environmental conditions inhibit AIA-derived FLP-2
354 signaling. However, the AIA response to acute pheromone presentation is likely to be mediated by the
355 fast ionotropic glutamate-gated GLC-3 chloride channel. Based on our epistasis analysis results, FLP-2
356 signaling is largely mediated by the slower-acting metabotropic MGL-1 receptor. Larvae are also
357 exposed to lower pheromone concentrations over longer timescales during dauer formation assays
358 compared to the microfluidics setup. Furthermore, larvae encounter other multimodal sensory cues
359 such as temperature and food during dauer formation assays, which might interact with and modulate
360 the neuronal response to pheromone. Thus, post-inhibitory activity rebounds driven by acute neuronal
361 inhibition might not actually be occurring during the actual diapause entry decision-making process.
362 While acute pheromone delivery is useful for identifying the valence of a neuron's response to the
363 stimulus, it is clearly insufficient to accurately determine larval neuronal dynamics over
364 developmentally-relevant timescales. Advances in long-term functional imaging of neurons in larvae
365 cultured in agarose microchambers might well be useful for this application (Bringmann, 2011; Turek et
366 al., 2015).

367 Neuropeptide signaling is an ancient inter-tissue communication mechanism that regulates
368 animal behavioral and physiological states (Elphick et al., 2018). In *C. elegans*, individual neuron
369 classes and non-neuronal tissue types express a constellation of neuropeptides and neuropeptide
370 receptors underscoring the vastness and complexity of extrasynaptic neurohormonal networks present
371 in a simple organism (Taylor et al., 2021). The arrested dauer organismal phenotype arises from
372 coordinated multi-tissue remodeling driven by individual fate decisions computed at the cellular level. In
373 this study, we discovered that developmentally-relevant sensory inputs likely spatially bifurcate

374 downstream of AIA-mediated FLP-2 signaling at the NPR-30 neuropeptide receptor, which is expressed
375 in the intestine in addition to other neuron classes and thus has the hallmarks of a fan-out circuit motif.
376 Future studies comparing the roles of NPR-30-mediated signaling between neuronal and intestinal cell
377 types during diapause entry might yield insights into the mechanisms of tissue-specific neuropeptide
378 modulation. Insulin/insulin-like growth factor (IGF) signaling is a similarly conserved inter-tissue
379 communication pathway (Garofalo, 2002; Murphy and Hu, 2013). The DAF-2 receptor tyrosine kinase is
380 the only insulin/IGF receptor encoded by the *C. elegans* genome and is expressed in the intestine and
381 nervous system (Hunt-Newbury et al., 2007; Kimura et al., 2011; Kimura et al., 1997). *daf-2* loss-of-
382 function mutants have an increased dauer formation phenotype indicating that the INS-1 ligand
383 antagonizes DAF-2 receptor signaling (Kimura et al., 1997). We have shown that FLP-2 and INS-1
384 mediate antagonistic signaling pathways during pheromone-induced diapause entry, and they likely
385 converge on intestinal cells that co-express NPR-30 and DAF-2. This discovery is concordant with the
386 intestine being a key target tissue in the diapause entry decision, and we have demonstrated a neural
387 pathway from sensory transduction to this target tissue (Hung et al., 2014).
388 Obesity is an increasingly prevalent disease characterized by excessive levels of body adiposity
389 and is itself a risk factor for other debilitating medical conditions such as cancer, diabetes, and heart
390 disease (Blüher, 2019). G-protein coupled receptors are important regulators of metabolism and energy
391 homeostasis, and mutations in genes encoding these metabotropic receptors are associated with
392 altered risk for developing obesity (Akbari et al., 2021; Oliveira de Souza et al., 2021). It is striking that
393 in the neural pathway regulating *C. elegans* larval developmental plasticity identified here, all receptors
394 involved are G-protein coupled metabotropic receptors (MGL-1, NPR-30, NPR-9). This highlights a
395 conserved role for metabotropic receptors in establishing and maintaining chronic metabolic and
396 physiological states, the dysfunction of which can have profound effects on an organism's life history.
397 The metabotropic glutamate receptor MGL-1 mediates foraging behavior and reproductive
398 plasticity in adult *C. elegans*, and is expressed in just four interneuron classes AIA, RMD, AIY, and
399 NSM (Jeong and Paik, 2017; López-Cruz et al., 2019). Here, we show that MGL-1 plays a critical role in
400 establishing an alternative larval phenotype over developmentally-relevant timescales by inhibiting
401 growth-promoting FLP-2 neuropeptide signaling. MGL-1 is similar in sequence to the mammalian group
402 II glutamate metabotropic receptors mGluR2 and mGluR3, which are expressed in the hypothalamus
403 and pituitary gland (Durand et al., 2008). When activated by glutamate binding, the group II mGluRs
404 inhibit cyclic AMP production as a result of their negative coupling to adenylyl cyclase resulting in
405 inhibition of the receptor-expressing neuron (Cartmell and Schoepp, 2000). In mammalian nervous
406 systems, the hypothalamus receives inputs from multiple sensory modalities and integrates this wide
407 range of information to drive appropriate behavioral and physiological responses (Saper and Lowell,

408 2014). In particular, the hypothalamic-pituitary axis of transmission mediates many aspects of growth,
409 development, and the response to stressful stimuli through neuroendocrine regulation (Saper and
410 Lowell, 2014). In these brain regions, glutamatergic neurotransmission via group II mGluRs inhibits the
411 release of neuroendocrine factors (Durand et al., 2008; Scaccianoce et al., 2003). Similarly in *C.*
412 *elegans*, we find that the AIA interneurons act as an integrative hub that translates inhibitory
413 glutamatergic neurotransmission from the sensory layer into downregulation of neuropeptidergic
414 signaling that ultimately impacts energy metabolism, reproductive physiology, and organismal
415 morphology.
416

417 **ACKNOWLEDGMENTS**
418 Some strains were provided by the CGC, which is funded by NIH Office of Research Infrastructure
419 Programs (P40 OD010440). WormBase provided key molecular and genetic information. Some strains
420 were provided by the lab of Dr. Shohei Mitani as part of the National Bioresource Project. Figure 1A
421 was created with BioRender.com.
422

423 **AUTHOR CONTRIBUTIONS**
424 Conceptualization – CMC, PWS. Methodology – CMC. Crude pheromone extraction and dauer
425 formation assays – CMC. Molecular cloning and transgenesis – CMC. Microscopy – CMC. CRISPR
426 mutagenesis – HP. Calcium imaging – MT, MS. Data analysis – CMC, MT, MS. CMC wrote the paper
427 with input from all authors. Funding acquisition – PWS, VV.
428

429 **FUNDING**
430 PWS, CMC, and HP were supported by NIH grants R24OD023041, UF1NS111697, and
431 R21MH115454. VV, MT, and MS were supported by a Burroughs Wellcome Fund Career Award at the
432 Scientific Interface and the American Federation for Aging Research.
433

434 **DECLARATION OF INTERESTS**
435 The authors declare no competing interests.
436

437 **FIGURE LEGENDS**
438 **Figure 1. AIA inhibition recapitulates the increased dauer formation phenotype of a *flp-2* mutant**.
439 (A) Schematic illustration showing different multimodal environmental inputs integrated by an L1 larva
440 during the diapause entry decision.

441 (B) Schematic illustration showing hierarchical organization of neural processing layers controlling *C.*
442 *elegans* behavior.
443 (C) Dauer formation assays for AIA::*HisCl1* animals grown on plates with and without histamine. N=9
444 population assays. Data represented as mean ± SEM, Welch's T-test, **p<0.01.
445 (D) Dauer formation assays for *flp-2(-)* mutants. N=5-6 population assays. Data represented as mean ±
446 SEM, Welch's T-test, *p<0.05.
447 (E) P*flp-2*::*GFP* colocalization with AIA-specific P*gcy-28*.d::*mCherry-H2B* marker in an L1 stage larva.
448
449 **Figure 2. AIA-derived FLP-2 promotes larval entry into the reproductive growth trajectory.**
450 (A) Dauer formation assays for AIA-specific *flp-2* cDNA expression in an *flp-2(-)* mutant background.
451 N=5 population assays. Data represented as mean ± SEM, ANOVA followed by Tukey HSD posthoc,
452 **p<0.01, n.s.=no significance.
453 (B) Dauer formation assays for AIA-specific *flp-2* cDNA overexpression. N=3 population assays. Data
454 represented as mean ± SEM, Welch's T-test, **p<0.01.
455 (C) P*flp-2*::*flp-2* cDNA::*mCherry* colocalization with AIA-specific P*gcy-28*.d::*GFP* in an L1 stage larva.
456 (D) FLP-2::mCherry accumulation within first pair of coelomocytes visualized with P*ofm-1*::*GFP* in an L1
457 stage larva.
458
459 **Figure 3. Pheromone activates ASK and ADL sensory neurons but inhibits downstream**
460 **AIA interneurons.**
461 (A) Schematic illustration of unweighted synaptic connections between ASK, ADL, AWA sensory
462 neurons and AIA.
463 (B) Dauer formation assays for ASK>*HisCl1* animals grown on plates with and without histamine. N=7-9
464 population assays. Data represented as mean ± SEM, Welch's T-test, ***p<0.001.
465 (C) ASK::*GCaMP6s* somatic average traces in response to pheromone delivery in microfluidics device.
466 L4 stage animals. Top panel – ASK (Left paired partner). Bottom panel – ASK (Right paired partner).
467 N=17 animals. Data represented as mean (thick black line) ± SEM (gray shading).
468 (D) Dauer formation assays for ADL::*HisCl1* animals grown on plates with and without histamine. N=8-
469 11 population assays. Data represented as mean ± SEM, Welch's T-test, *p<0.05.
470 (E) ADL::*GCaMP6s* somatic average traces in response to pheromone delivery in microfluidics device.
471 L4 stage animals. Top panel – ADL (Left paired partner). Bottom panel – ADL (Right paired partner).
472 N=17 animals. Data represented as mean (thick black line) ± SEM (gray shading).
473 (F) AIA::*GCaMP6s* process average trace in response to pheromone delivery in microfluidics device. L4
474 stage animals. N=5 animals. Data represented as mean (thick black line) ± SEM (gray shading).

475 (G) Dauer formation assays for N2 animals grown in presence of 2 µL ethanol or 2 µL 1:1000 diacetyl
476 diluted in ethanol. N=4 population assays. Data represented as mean ± SEM, Welch's T-test, n.s.=no
477 significance.
478
479 **Figure 4. FLP-2 signaling is inhibited by upstream glutamatergic transmission via the**
480 **metabotropic glutamate receptor MGL-1**
481 (A) Percentage of full dauers (red), partial dauers (gray), and reproductive adults (blue) formed during
482 dauer formation assays for N2 and *glc-3(-)* mutants. N=146 animals (N2) and 135 animals (*glc-3(-)*), 2
483 trials per genotype.
484 (B) Dauer formation assays for *flp-2(-); glc-3(-)* double mutant genetic epistasis analysis. N=3-4
485 population assays. Data represented as mean ± SEM, ANOVA followed by Tukey HSD posthoc,
486 *p<0.05, **p<0.01.
487 (C) Dauer formation assays for *flp-2(-); mgl-1(-)* double mutant genetic epistasis analysis. N=3-4
488 population assays. Data represented as mean ± SEM, ANOVA followed by Tukey HSD posthoc,
489 *p<0.05, ***p<0.001, n.s.=no significance.
490
491 **Figure 5. The broadly-expressed neuropeptide receptor NPR-30 is downstream of FLP-2**
492 **signaling.**
493 (A) Dauer formation assays for *flp-2(-); frpr-18(-)* double mutant genetic epistasis analysis. N=6-7
494 population assays. Data represented as mean ± SEM, ANOVA followed by Tukey HSD posthoc,
495 **p<0.01, ***p<0.001.
496 (B) Dauer formation assays for *npr-30(-)* suppression of AIA::*flp-2* cDNA overexpression. Only
497 transgenic animals counted. N=4-8 population assays. Data represented as mean ± SEM, ANOVA
498 followed by Tukey HSD posthoc, *p<0.05, ***p<0.001, n.s.=no significance.
499 (C) Representative image of *npr-30* translational GFP reporter (PS9109) expression in an L1 stage
500 larva. GFP expression present in nervous system and intestine. Left panel – GFP channel only. Right
501 panel – GFP and DIC channels merge.
502 (D) Representative image of *npr-30* translational GFP reporter (PS9152) expression in an L1 stage
503 larva. Strain injected with lower GFP reporter plasmid concentration than (C) to enable better
504 visualization of motor neurons located along the ventral side of the animal's body. GFP is expressed in
505 sensory neurons (white arrowhead pointing at dendritic processes extending towards nose tip),
506 interneurons, and motor neurons (white asterisk).

507 (E) Representative image showing AIA-specific P*gcy-28.d*::*mCherry-H2B* does not colocalize with an
508 *npr-30* translational GFP reporter in an L1 stage larva. Top panel – GFP and mCherry channels merge.
509 Bottom panel – GFP, mCherry, and DIC channels merge.
510
511 **Figure 6. Insulin-like growth factor INS-1 and FLP-2 have antagonistic roles in developmental**
512 **decision-making.**
513 (A) Dauer formation assays for *flp-2(-); ins-1(-)* double mutant genetic epistasis analysis. N=3-4
514 population assays. Data represented as mean ± SEM, ANOVA followed by Tukey HSD posthoc,
515 **p<0.01, ***p<0.001.
516 (B) Dauer formation assays for AIA-specific *ins-1* cDNA expression in an *ins-1(-)* mutant background.
517 N=4 population assays. Data represented as mean ± SEM, ANOVA followed by Tukey HSD posthoc,
518 ***p<0.001, n.s.=no significance.
519 (C) Schematic model showing antagonistic relationship between FLP-2 and INS-1 signaling during
520 diapause entry.
521
522 **Figure 7. AIB interneurons and their neuropeptide receptor NPR-9/GALR2 promote diapause**
523 **entry.**
524 (A) Dauer formation assays for AIB>*HisCl1* animals grown on plates with and without histamine. N=7
525 population assays. Data represented as mean ± SEM, Welch's T-test, ***p<0.001.
526 (B) Dauer formation assays for *flp-2(-); npr-9(-)* double mutant genetic epistasis analysis. N=2-4
527 population assays. Data represented as mean ± SEM, ANOVA followed by Tukey HSD posthoc,
528 *p<0.05, ***p<0.001, n.s.=no significance.
529 (C) AIB::*GCaMP6s* process average trace in response to pheromone delivery in microfluidics device.
530 L4 stage animals. N=13 animals. Data represented as mean (thick black line) ± SEM (gray shading).
531
532 **Figure 8: AIA controls a neuropeptide switch between different larval developmental**
533 **trajectories.**
534 (A and B) Schematic model of AIA-derived FLP-2 signaling pathway under different environmental
535 conditions: (A) Reproductive growth conditions and (B) Dauer-inducing conditions.
536 (C) Schematic model of neural circuit mediating the diapause entry decision including pheromone-
537 sensing neurons and interneurons identified in this study.
538
539 **Supplementary Figure 1: Intestine-specific *flp-2* cDNA expression does not rescue *flp-2(-)***
540 **mutant increased dauer formation phenotype.**

541 Dauer formation assays for intestine-specific *flp-2* cDNA expression in an *flp-2(-)* mutant background.
542 N=3-4 population assays. Data represented as mean ± SEM, ANOVA followed by Tukey HSD posthoc,
543 *p<0.05, n.s.=no significance.
544
545 **Supplementary Figure 2. AIA soma GCaMP response to pheromone delivery.**
546 AIA::*GCaMP6s* somatic average traces in response to pheromone delivery in microfluidics device. L4
547 stage animals. Top panel – AIA (Left paired partner). Bottom panel – AIA (Right paired partner). N=5
548 animals. Data represented as mean (thick black line) ± SEM (gray shading).
549
550 **Supplementary Figure 3. *mgl-1*(*tm1811*) deletion allele has a decreased dauer formation**
551 **phenotype.**
552 Dauer formation assays for *mgl-1*(*tm1811*) mutants. N=4 population assays. Data represented as mean
553 ± SEM, Welch's T-test, **p<0.01.
554
555 **Supplementary Figure 4. AIB soma GCaMP response to pheromone delivery.**
556 AIB::*GCaMP6s* somatic average traces in response to pheromone delivery in microfluidics device. L4
557 stage animals. Top panel – AIB (Left paired partner). Bottom panel – AIB (Right paired partner). N=13
558 animals. Data represented as mean (thick black line) ± SEM (gray shading).
559

560 ## MATERIALS AND METHODS

561 **Animal maintenance and strains**

562 Animals were cultivated at 21°C on standard nematode growth media (NGM) plates seeded with
563 *Escherichia coli* OP50 cultured in Luria-Bertani (LB) broth. The following strains were used in this study:
564 **N2** (Bristol)
565 **PS8919**: *syEx1777*[P*flp-2*::*GFP*, P*gcy-28*.d::*mCherry-H2B*, P*ofm-1*::*RFP*]
566 **PS9101**: *syIs759*[P*gcy-28*.d::*HisCl1*::SL2::*GFP*, P*flp-2*::*flp-2* cDNA::*mCherry*, P*ofm-1*::*GFP*]
567 **PS7370**: *flp-2*(*ok3351*)
568 **PS8968**: *flp-2*(*ok3351*); *syEx1755*[P*flp-2*::*flp-2* cDNA::SL2::*GFP*, P*ofm-1*::*RFP*]
569 **PS9150**: *flp-2*(*ok3351*); *syEx1866*[P*ges-1*::*flp-2* cDNA::SL2::*GFP*, P*ofm-1*::*RFP*]
570 **PS8735**: *syEx1755*[P*flp-2*::*flp-2* cDNA::SL2::*GFP*, P*ofm-1*::*RFP*]
571 **PS7866**: *syIs493*[P*sra-9*::*cGAL*, P*ofm-1*::*RFP*]; *syIs371*[*UAS*::*HisCl1*::SL2::*GFP*, P*ofm-1*::*GFP*]
572 **PS8159**: *syIs540*[P*npr-9*::*cGAL*, P*ofm-1*::*RFP*]; *syIs371*[*UAS*::*HisCl1*::SL2::*GFP*, P*ofm-1*::*GFP*]
573 **PS9006**: *syEx1811*[P*sre-1*::*HisCl1*::SL2::*GFP*, P*ofm-1*::*RFP*]
574 **PS8955**: *syEx1793*[P*sra-9*::*GCaMP6s*, P*sre-1*::*GCaMP6s*, P*gcy-28*.d::*GCaMP6s*]

575 **PS9111**: *syIs761*[P*gcy-28*.d::*GCaMP6s*, P*myo-2*::*mCherry*]
576 **PS8162**: *syIs543*[P*npr-9*::*GCaMP6s*, P*ofm-1*::*RFP*]
577 **RB594**: *glc-3*(*ok321*)
578 **PS8586**: *npr-9*(*sy1417*)
579 **PS8628:** *flp-2*(*ok3351*); *npr-9*(*sy1429*)
580 **PS9192:** *mgl-1*(*sy1623*)
581 **PS9193**: *flp-2*(*ok3351*); *mgl-1*(*sy1624*)
582 **FX01811**: *mgl-1(tm1811)*
583 **PS7624:** *frpr-18*(*ok2698*)
584 **PS7831**: *flp-2*(*ok3351*); *frpr-18*(*ok2698*)
585 **FX06617**: *npr-30*(*tm6617*)
586 **PS8931**: *npr-30*(*tm6617*); *syEx1755*[P*flp-2*::*flp-2* cDNA::SL2::*GFP*, P*ofm-1*::*RFP*]
587 **FX01888:** *ins-1*(*tm1888*)
588 **PS9137:** *flp-2*(*ok3351*); *ins-1*(*tm1888*)
589 **PS9147**: *ins-1*(*tm1888*); *syEx1863*[P*gcy-28*.d::*ins-1* cDNA::SL2::*mCherry-H2B*, P*ofm-1*::*RFP*]
590 **PS9109**: *npr-30*(*tm6617*); *syEx1844*[P*npr-30*::*npr-30* genomic DNA::SL2::*GFP*, P*tax-4*::*mCherry-H2B*,
591 P*ofm-1*::*RFP*]
592 **PS9152**: *npr-30*(*tm6617*); *syEx1868*[P*npr-30*::*npr-30* genomic DNA::SL2::*GFP*, P*gcy-28*.d::*mCherry-*
593 *H2B*, P*ofm-1*::*RFP*]
594
595 **Molecular biology and transgenesis**
596 *flp-2 and ins-1* cDNA were PCR amplified from N2 cDNA library. Promoters and *npr-30* genomic
597 DNA were PCR amplified from N2 genomic DNA library. *Drosophila HisCl1* was PCR amplified from
598 pJL046 (Wang et al., 2017). Constructs were inserted into pSM *GFP*, pSM *mCherry-H2B*, or pSM
599 *GCaMP6s* vector backbone using HiFi Assembly or restriction cloning. ASK>*HisCl1* and AIB>*HisCl1*
600 neuronal silencing strains were generated by placing a *15xUAS*::*HisCl1*::SL2::*GFP* effector under the
601 control of ASK and AIB-specific drivers respectively (Wang et al., 2017).
602 Transgenic strains were generated by microinjection of plasmids with co-injection markers into
603 adult worms. Plasmids were injected at 10-50 ng/μL. Co-injection markers were injected at: P*myo-*
604 *2*::*mCherry* (0.5 ng/μL), P*ofm-1*::*RFP* (40 ng/μL), P*ofm-1*::*GFP* (30-40 ng/μL). 1 kb DNA ladder was
605 used as a filler to bring final DNA concentration to 200 ng/μL.
606
607 **CRISPR mutagenesis**

608 CRISPR mutagenesis was performed as described in previously described(Wang et al., 2018).
609 Briefly, a 43-base-pair universal STOP-IN cassette was inserted near the 5' end of the target gene to
610 disrupt translation. Independent F2 homozygous animals were isolated using PCR detection and
611 confirmed with Sanger sequencing.
612
613 **Pheromone-induced dauer formation assays**
614 Crude dauer pheromone extract was prepared as previously described (Schroeder and Flatt,
615 2014). To control for differences in pheromone potency between batches, a pheromone dose response
616 curve was generated for each batch and the pheromone volume that yielded 50% dauer formation
617 under the experimental conditions described below was selected for dauer formation assays. 8% (w/v)
618 heat-killed OP50 was made by washing bacteria from an overnight culture with virgin S-basal,
619 resuspending with virgin S-basal, and killing at 95-100°C. The afternoon before experiments, L4 worms
620 were picked from well-fed stock plates onto seeded plates and grown overnight at 21°C. Pheromone of
621 desired volume was placed at the center of 35 mm Petri dishes and 2 mL of NGM agar without peptone
622 was poured into each plate. Plates were dried overnight on benchtop at 21°C. On the day of
623 experiments, pheromone plates were seeded with 2 µL heat-killed OP50 and adults animals were
624 allowed to lay 60-70 eggs per plate. Adults were then picked off and 18 µL of heat-killed OP50 added to
625 the plates. Once the food patch had completely dried, plates were sealed with parafilm and placed in a
626 25.5°C incubator for 72 hours. The number of dauers and non-dauers per plate were counted and the
627 Dauer Formation Index (DFI) per plate calculated using the following formula:
628
629 $$\text{DFI} = \frac{\text{No. of Dauers} - \text{No. of Non-dauers}}{\text{No. of Dauers} + \text{No. of Non-dauers}}$$
630
631 To make histamine plates, histamine dihydrochloride powder was mixed into NGM agar at
632 ~50°C to a final concentration of 10 mM and poured into Petri dishes with pheromone.
633 For dauer formation assays with diacetyl, assays were set up as described above. Before
634 parafilming, 2 µL of 200 proof ethanol or 2 µL or 1:1000 diacetyl diluted in ethanol was added to the
635 side of the food patch.
636 For experiments using extrachromosomal array transgenic lines, lines that had 70-80% array
637 transmission rates were selected for population assays. All animals on each plate were counted unless
638 noted otherwise. At least 3 population assays were completed for each control and genotype/treatment
639 (except for N2 controls in Figure 7B), with each assay containing 60-70 animals. Control and
640 genotype/treatment plates were always assayed simultaneously under the same conditions for
641 comparisons.

642
643 **Microscopy**

644 Animals were immobilized with 50 mM sodium azide on 2% agarose pads. Slides were imaged
645 under a ZEISS Imager.Z2 microscope attached to a Axiocam 506 mono camera capture source.
646 Images were processed using ZenPro software.
647

648 **Calcium imaging**

649 *Microfluidic device fabrication*

650 We designed a 2-layer microfluidic chip capable of delivering sequences of stimuli with a
651 worm trap suitable for housing worms at L4 larval stage. The chip was designed in AutoCAD software,
652 and sent to CAD/Art Services, Inc to print the photomask. Photolithography in a clean room was
653 performed on a silicon wafer to make the 2-layer mold from the photomask. For the first layer, which
654 included the worm trap, SU-8 2025 was spin coated on the silicon wafer at 4000 rpm to achieve 25 µm
655 thickness. For the second layer, the same photoresist was spin coated at 1250 rpm for a thickness of
656 70 µm. Polydimethylsiloxane (PDMS) was poured over the mold and cured on a 90˚C hotplate to
657 solidify. Each PDMS chip was then punched with a 1 mm biopsy punch and was bonded to a cover
658 slip using a handheld corona treater.
659

660 *Microfluidic experiment design*

661 L4 stage animals were assayed and all experiments were conducted at 20˚C. We chose 3
662 stimuli for the experiment: 10% (v/v) crude pheromone extract diluted in CTX buffer (5 mM
663 KH_2PO_4/K_2HPO_4 pH 6, 1 mM $CaCl_2$ and 1 mM $MgSO_4$, 50 mM NaCl) as the main stimulus, CTX buffer
664 as the control stimulus, and 0.01 mM Fluorescein to confirm chemical delivery. Each stimulus interval
665 was 15 seconds, sufficient time to capture the rise and fall of calcium transients. Stimulus interval was
666 then followed by a 30-second CTX buffer interval to give neurons enough time to return to baseline and
667 be ready for the next stimulus.
668

669 *Data Analysis*

670 For each animal, fluorescence was captured at 4 volumes/second, 25 z-slices/volume and 1.2
671 µm/slice and average background intensity was subtracted from each volume. To measure calcium
672 activity of the neuron's soma, average intensity of pixels within a 3.2 µm x 3.2 µm x 3.6 µm volume
673 around the center of the soma was calculated. To extract calcium activity of neuron processes, a 38 µm
674 x 38 µm x 24 µm rectangular volume surrounding the processes were identified at each timepoint,

675 pixels from the soma were removed from the volume and the average intensity of the remaining pixels
676 were calculated. F_0 was defined as average intensity during the 5-second window before the delivery of
677 pheromone.
678

679 **STATISTICAL ANALYSIS**

680 For dauer formation assays, unpaired Welch's T-test or ANOVA followed by Tukey HSD
681 posthoc analysis were used to determine statistically significant differences between groups. All
682 statistical analyses were performed in R. All plots were generated in Python.
683

684 **LITERATURE CITED**

685 Akbari, P., Gilani, A., Sosina, O., Kosmicki, J.A., Khrimian, L., Fang, Y.Y., Persaud, T., Garcia, V.,
686 Sun, D., Li, A., et al. (2021). Sequencing of 640,000 exomes identifies GPR75 variants
687 associated with protection from obesity. Science *373*. 10.1126/science.abf8683.
688 Ashrafi, K. (2007). Obesity and the regulation of fat metabolism. WormBook, 1-20.
689 10.1895/wormbook.1.130.1.
690 Bargmann, C.I., Hartwieg, E., and Horvitz, H.R. (1993). Odorant-selective genes and neurons mediate
691 olfaction in C. elegans. Cell *74*, 515-527. 10.1016/0092-8674(93)80053-h.
692 Bargmann, C.I., and Horvitz, H.R. (1991). Control of larval development by chemosensory neurons in
693 Caenorhabditis elegans. Science *251*, 1243-1246. 10.1126/science.2006412.
694 Beldade, P., Mateus, A.R., and Keller, R.A. (2011). Evolution and molecular mechanisms of adaptive
695 developmental plasticity. Mol Ecol *20*, 1347-1363. 10.1111/j.1365-294X.2011.05016.x.
696 Bendena, W.G., Boudreau, J.R., Papanicolaou, T., Maltby, M., Tobe, S.S., and Chin-Sang, I.D. (2008).
697 A Caenorhabditis elegans allatostatin/galanin-like receptor NPR-9 inhibits local search behavior
698 in response to feeding cues. Proc Natl Acad Sci U S A *105*, 1339-1342.
699 10.1073/pnas.0709492105.
700 Bento, G., Ogawa, A., and Sommer, R.J. (2010). Co-option of the hormone-signalling module
701 dafachronic acid-DAF-12 in nematode evolution. Nature *466*, 494-497. 10.1038/nature09164.
702 Blüher, M. (2019). Obesity: global epidemiology and pathogenesis. Nature Reviews Endocrinology *15*,
703 288-298. 10.1038/s41574-019-0176-8.
704 Brakefield, P.M., Kesbeke, F., and Koch, P.B. (1998). The regulation of phenotypic plasticity of
705 eyespots in the butterfly Bicyclus anynana. Am Nat *152*, 853-860. 10.1086/286213.
706 Bringmann, H. (2011). Agarose hydrogel microcompartments for imaging sleep- and wake-like behavior
707 and nervous system development in Caenorhabditis elegans larvae. J Neurosci Methods *201*, 78-
708 88. 10.1016/j.jneumeth.2011.07.013.
709 Brockie, P.J., Madsen, D.M., Zheng, Y., Mellem, J., and Maricq, A.V. (2001). Differential expression of
710 glutamate receptor subunits in the nervous system of Caenorhabditis elegans and their regulation
711 by the homeodomain protein UNC-42. J Neurosci *21*, 1510-1522. 10.1523/jneurosci.21-05-
712 01510.2001.
713 Butcher, R.A., Ragains, J.R., Kim, E., and Clardy, J. (2008). A potent dauer pheromone component in
714 Caenorhabditis elegans that acts synergistically with other components. Proc Natl Acad Sci U S
715 A *105*, 14288-14292. 10.1073/pnas.0806676105.

716 Cartmell, J., and Schoepp, D.D. (2000). Regulation of neurotransmitter release by metabotropic
717 glutamate receptors. J Neurochem *75*, 889-907. 10.1046/j.1471-4159.2000.0750889.x.
718 Cassada, R.C., and Russell, R.L. (1975). The dauerlarva, a post-embryonic developmental variant of the
719 nematode Caenorhabditis elegans. Dev Biol *46*, 326-342. 10.1016/0012-1606(75)90109-8.
720 Chalasani, S.H., Kato, S., Albrecht, D.R., Nakagawa, T., Abbott, L.F., and Bargmann, C.I. (2010).
721 Neuropeptide feedback modifies odor-evoked dynamics in Caenorhabditis elegans olfactory
722 neurons. Nat Neurosci *13*, 615-621. 10.1038/nn.2526.
723 Chase, D.L., and Koelle, M.R. (2007). Biogenic amine neurotransmitters in C. elegans. WormBook, 1-
724 15. 10.1895/wormbook.1.132.1.
725 Chen, T.-W., Wardill, T.J., Sun, Y., Pulver, S.R., Renninger, S.L., Baohan, A., Schreiter, E.R., Kerr,
726 R.A., Orger, M.B., Jayaraman, V., et al. (2013). Ultrasensitive fluorescent proteins for imaging
727 neuronal activity. Nature *499*, 295-300. 10.1038/nature12354.
728 Dillon, J., Hopper, N.A., Holden-Dye, L., and O'Connor, V. (2006). Molecular characterization of the
729 metabotropic glutamate receptor family in Caenorhabditis elegans. Biochem Soc Trans *34*, 942-
730 948. 10.1042/bst0340942.
731 Dobosiewicz, M., Liu, Q., and Bargmann, C.I. (2019). Reliability of an interneuron response depends on
732 an integrated sensory state. Elife *8*. 10.7554/eLife.50566.
733 Durand, D., Pampillo, M., Caruso, C., and Lasaga, M. (2008). Role of metabotropic glutamate receptors
734 in the control of neuroendocrine function. Neuropharmacology *55*, 577-583.
735 10.1016/j.neuropharm.2008.06.022.
736 Elphick, M.R., Mirabeau, O., and Larhammar, D. (2018). Evolution of neuropeptide signalling systems.
737 J Exp Biol *221*. 10.1242/jeb.151092.
738 Fares, H., and Greenwald, I. (2001). Genetic analysis of endocytosis in Caenorhabditis elegans:
739 coelomocyte uptake defective mutants. Genetics *159*, 133-145. 10.1093/genetics/159.1.133.
740 Faumont, S., Lindsay, T.H., and Lockery, S.R. (2012). Neuronal microcircuits for decision making in C.
741 elegans. Curr Opin Neurobiol *22*, 580-591. 10.1016/j.conb.2012.05.005.
742 Fujiwara, M., Aoyama, I., Hino, T., Teramoto, T., and Ishihara, T. (2016). Gonadal Maturation Changes
743 Chemotaxis Behavior and Neural Processing in the Olfactory Circuit of Caenorhabditis elegans.
744 Curr Biol *26*, 1522-1531. 10.1016/j.cub.2016.04.058.
745 Garofalo, R.S. (2002). Genetic analysis of insulin signaling in Drosophila. Trends Endocrinol Metab *13*,
746 156-162. 10.1016/s1043-2760(01)00548-3.
747 Golden, J.W., and Riddle, D.L. (1982). A pheromone influences larval development in the nematode
748 Caenorhabditis elegans. Science *218*, 578-580. 10.1126/science.6896933.
749 Golden, J.W., and Riddle, D.L. (1984). The Caenorhabditis elegans dauer larva: developmental effects
750 of pheromone, food, and temperature. Dev Biol *102*, 368-378. 10.1016/0012-1606(84)90201-x.
751 Greer, E.R., Pérez, C.L., Van Gilst, M.R., Lee, B.H., and Ashrafi, K. (2008). Neural and molecular
752 dissection of a C. elegans sensory circuit that regulates fat and feeding. Cell Metab *8*, 118-131.
753 10.1016/j.cmet.2008.06.005.
754 Hallem, E.A., Dillman, A.R., Hong, A.V., Zhang, Y., Yano, J.M., DeMarco, S.F., and Sternberg, P.W.
755 (2011). A sensory code for host seeking in parasitic nematodes. Curr Biol *21*, 377-383.
756 10.1016/j.cub.2011.01.048.
757 Hendricks, M., Ha, H., Maffey, N., and Zhang, Y. (2012). Compartmentalized calcium dynamics in a C.
758 elegans interneuron encode head movement. Nature *487*, 99-103. 10.1038/nature11081.
759 Horoszok, L., Raymond, V., Sattelle, D.B., and Wolstenholme, A.J. (2001). GLC-3: a novel fipronil and
760 BIDN-sensitive, but picrotoxinin-insensitive, L-glutamate-gated chloride channel subunit from
761 Caenorhabditis elegans. Br J Pharmacol *132*, 1247-1254. 10.1038/sj.bjp.0703937.

762 Huang, Z., Huang, L., Waters, M.J., and Chen, C. (2020). Insulin and Growth Hormone Balance:
763 Implications for Obesity. Trends Endocrinol Metab *31*, 642-654. 10.1016/j.tem.2020.04.005.
764 Hung, W.L., Wang, Y., Chitturi, J., and Zhen, M. (2014). A Caenorhabditis elegans developmental
765 decision requires insulin signaling-mediated neuron-intestine communication. Development *141*,
766 1767-1779. 10.1242/dev.103846.
767 Hunt-Newbury, R., Viveiros, R., Johnsen, R., Mah, A., Anastas, D., Fang, L., Halfnight, E., Lee, D.,
768 Lin, J., Lorch, A., et al. (2007). High-throughput in vivo analysis of gene expression in
769 Caenorhabditis elegans. PLoS Biol *5*, e237. 10.1371/journal.pbio.0050237.
770 Jang, H., Kim, K., Neal, S.J., Macosko, E., Kim, D., Butcher, R.A., Zeiger, D.M., Bargmann, C.I., and
771 Sengupta, P. (2012). Neuromodulatory state and sex specify alternative behaviors through
772 antagonistic synaptic pathways in C. elegans. Neuron *75*, 585-592.
773 10.1016/j.neuron.2012.06.034.
774 Janzen, F.J., and Paukstis, G.L. (1991). Environmental sex determination in reptiles: ecology, evolution,
775 and experimental design. Q Rev Biol *66*, 149-179. 10.1086/417143.
776 Jeong, H., and Paik, Y.K. (2017). MGL-1 on AIY neurons translates starvation to reproductive plasticity
777 via neuropeptide signaling in Caenorhabditis elegans. Dev Biol *430*, 80-89.
778 10.1016/j.ydbio.2017.08.014.
779 Jeong, P.-Y., Jung, M., Yim, Y.-H., Kim, H., Park, M., Hong, E., Lee, W., Kim, Y.H., Kim, K., and
780 Paik, Y.-K. (2005). Chemical structure and biological activity of the Caenorhabditis elegans
781 dauer-inducing pheromone. Nature *433*, 541-545. 10.1038/nature03201.
782 Kelly, S.A., Panhuis, T.M., and Stoehr, A.M. (2012). Phenotypic plasticity: molecular mechanisms and
783 adaptive significance. Compr Physiol *2*, 1417-1439. 10.1002/cphy.c110008.
784 Kim, K., and Li, C. (2004). Expression and regulation of an FMRFamide-related neuropeptide gene
785 family in Caenorhabditis elegans. J Comp Neurol *475*, 540-550. 10.1002/cne.20189.
786 Kim, K., Sato, K., Shibuya, M., Zeiger, D.M., Butcher, R.A., Ragains, J.R., Clardy, J., Touhara, K., and
787 Sengupta, P. (2009). Two chemoreceptors mediate developmental effects of dauer pheromone in
788 C. elegans. Science *326*, 994-998. 10.1126/science.1176331.
789 Kimura, K.D., Riddle, D.L., and Ruvkun, G. (2011). The C. elegans DAF-2 insulin-like receptor is
790 abundantly expressed in the nervous system and regulated by nutritional status. Cold Spring
791 Harb Symp Quant Biol *76*, 113-120. 10.1101/sqb.2011.76.010660.
792 Kimura, K.D., Tissenbaum, H.A., Liu, Y., and Ruvkun, G. (1997). daf-2, an insulin receptor-like gene
793 that regulates longevity and diapause in Caenorhabditis elegans. Science *277*, 942-946.
794 10.1126/science.277.5328.942.
795 Klass, M., and Hirsh, D. (1976). Non-ageing developmental variant of Caenorhabditis elegans. Nature
796 *260*, 523-525. 10.1038/260523a0.
797 Kodama, E., Kuhara, A., Mohri-Shiomi, A., Kimura, K.D., Okumura, M., Tomioka, M., Iino, Y., and
798 Mori, I. (2006). Insulin-like signaling and the neural circuit for integrative behavior in C.
799 elegans. Genes Dev *20*, 2955-2960. 10.1101/gad.1479906.
800 Laforsch, C., Beccara, L., and Tollrian, R. (2006). Inducible defenses: The relevance of chemical alarm
801 cues in Daphnia. Limnology and Oceanography *51*, 1466-1472.
802 https://doi.org/10.4319/lo.2006.51.3.1466.
803 Larsen, M.J., Lancheros, E.R., Williams, T., Lowery, D.E., Geary, T.G., and Kubiak, T.M. (2013).
804 Functional expression and characterization of the C. elegans G-protein-coupled FLP-2 Receptor
805 (T19F4.1) in mammalian cells and yeast. Int J Parasitol Drugs Drug Resist *3*, 1-7.
806 10.1016/j.ijpddr.2012.10.002.

807 Lee, H., Choi, M.K., Lee, D., Kim, H.S., Hwang, H., Kim, H., Park, S., Paik, Y.K., and Lee, J. (2011).
808 Nictation, a dispersal behavior of the nematode Caenorhabditis elegans, is regulated by IL2
809 neurons. Nat Neurosci *15*, 107-112. 10.1038/nn.2975.
810 Lee, J.S., Shih, P.Y., Schaedel, O.N., Quintero-Cadena, P., Rogers, A.K., and Sternberg, P.W. (2017).
811 FMRFamide-like peptides expand the behavioral repertoire of a densely connected nervous
812 system. Proc Natl Acad Sci U S A *114*, E10726-e10735. 10.1073/pnas.1710374114.
813 López-Cruz, A., Sordillo, A., Pokala, N., Liu, Q., McGrath, P.T., and Bargmann, C.I. (2019). Parallel
814 Multimodal Circuits Control an Innate Foraging Behavior. Neuron *102*, 407-419.e408.
815 10.1016/j.neuron.2019.01.053.
816 Macosko, E.Z., Pokala, N., Feinberg, E.H., Chalasani, S.H., Butcher, R.A., Clardy, J., and Bargmann,
817 C.I. (2009). A hub-and-spoke circuit drives pheromone attraction and social behaviour in C.
818 elegans. Nature *458*, 1171-1175. 10.1038/nature07886.
819 McGrath, P.T., Xu, Y., Ailion, M., Garrison, J.L., Butcher, R.A., and Bargmann, C.I. (2011). Parallel
820 evolution of domesticated Caenorhabditis species targets pheromone receptor genes. Nature *477*,
821 321-325. 10.1038/nature10378.
822 Michimae, H., and Wakahara, M. (2001). Factors Which Affect the Occurrence of Cannibalism and the
823 Broad-Headed "Cannibal" Morph in Larvae of the Salamander Hynobius retardatus. Behavioral
824 Ecology and Sociobiology *50*, 339-345.
825 Moczek, A.P., and Emlen, D.J. (2000). Male horn dimorphism in the scarab beetle, Onthophagus taurus:
826 do alternative reproductive tactics favour alternative phenotypes? Anim Behav *59*, 459-466.
827 10.1006/anbe.1999.1342.
828 Murphy, C.T., and Hu, P.J. (2013). Insulin/insulin-like growth factor signaling in C. elegans.
829 WormBook, 1-43. 10.1895/wormbook.1.164.1.
830 Nijhout, H.F. (2003). Development and evolution of adaptive polyphenisms. Evol Dev *5*, 9-18.
831 10.1046/j.1525-142x.2003.03003.x.
832 Oliveira de Souza, C., Sun, X., and Oh, D. (2021). Metabolic Functions of G Protein-Coupled Receptors
833 and β-Arrestin-Mediated Signaling Pathways in the Pathophysiology of Type 2 Diabetes and
834 Obesity. Front Endocrinol (Lausanne) *12*, 715877. 10.3389/fendo.2021.715877.
835 Pereira, L., Kratsios, P., Serrano-Saiz, E., Sheftel, H., Mayo, A.E., Hall, D.H., White, J.G., LeBoeuf, B.,
836 Garcia, L.R., Alon, U., and Hobert, O. (2015). A cellular and regulatory map of the cholinergic
837 nervous system of C. elegans. Elife *4*. 10.7554/eLife.12432.
838 Pfennig, D.W. (1992). Polyphenism in Spadefoot Toad Tadpoles as a Locally Adjusted Evolutionarily
839 Stable Strategy. Evolution *46*, 1408-1420. 10.1111/j.1558-5646.1992.tb01133.x.
840 Podrabsky, J.E., and Hand, S.C. (1999). The bioenergetics of embryonic diapause in an annual killifish,
841 austrofundulus limnaeus. J Exp Biol *202 (Pt 19)*, 2567-2580.
842 Pokala, N., Liu, Q., Gordus, A., and Bargmann, C.I. (2014). Inducible and titratable silencing of
843 Caenorhabditis elegans neurons in vivo with histamine-gated chloride channels. Proceedings of
844 the National Academy of Sciences *111*, 2770-2775. 10.1073/pnas.1400615111.
845 Pungaliya, C., Srinivasan, J., Fox, B.W., Malik, R.U., Ludewig, A.H., Sternberg, P.W., and Schroeder,
846 F.C. (2009). A shortcut to identifying small molecule signals that regulate behavior and
847 development in Caenorhabditis elegans. Proceedings of the National Academy of Sciences *106*,
848 7708-7713. 10.1073/pnas.0811918106.
849 Putrenko, I., Zakikhani, M., and Dent, J.A. (2005). A family of acetylcholine-gated chloride channel
850 subunits in Caenorhabditis elegans. J Biol Chem *280*, 6392-6398. 10.1074/jbc.M412644200.
851 Saper, C.B., and Lowell, B.B. (2014). The hypothalamus. Curr Biol *24*, R1111-1116.
852 10.1016/j.cub.2014.10.023.

853 Scaccianoce, S., Matrisciano, F., Del Bianco, P., Caricasole, A., Di Giorgi Gerevini, V., Cappuccio, I.,
854 Melchiorri, D., Battaglia, G., and Nicoletti, F. (2003). Endogenous activation of group-II
855 metabotropic glutamate receptors inhibits the hypothalamic-pituitary-adrenocortical axis.
856 Neuropharmacology *44*, 555-561. 10.1016/s0028-3908(03)00027-3.
857 Schackwitz, W.S., Inoue, T., and Thomas, J.H. (1996). Chemosensory neurons function in parallel to
858 mediate a pheromone response in C. elegans. Neuron *17*, 719-728. 10.1016/s0896-
859 6273(00)80203-2.
860 Schroeder, N.E., and Flatt, K.M. (2014). In vivo imaging of Dauer-specific neuronal remodeling in C.
861 elegans. J Vis Exp, e51834. 10.3791/51834.
862 Serrano-Saiz, E., Poole, R.J., Felton, T., Zhang, F., De La Cruz, E.D., and Hobert, O. (2013). Modular
863 control of glutamatergic neuronal identity in C. elegans by distinct homeodomain proteins. Cell
864 *155*, 659-673. 10.1016/j.cell.2013.09.052.
865 Shinkai, Y., Yamamoto, Y., Fujiwara, M., Tabata, T., Murayama, T., Hirotsu, T., Ikeda, D.D.,
866 Tsunozaki, M., Iino, Y., Bargmann, C.I., et al. (2011). Behavioral choice between conflicting
867 alternatives is regulated by a receptor guanylyl cyclase, GCY-28, and a receptor tyrosine kinase,
868 SCD-2, in AIA interneurons of Caenorhabditis elegans. J Neurosci *31*, 3007-3015.
869 10.1523/jneurosci.4691-10.2011.
870 Sze, J.Y., Victor, M., Loer, C., Shi, Y., and Ruvkun, G. (2000). Food and metabolic signalling defects in
871 a Caenorhabditis elegans serotonin-synthesis mutant. Nature *403*, 560-564. 10.1038/35000609.
872 Taylor, S.R., Santpere, G., Weinreb, A., Barrett, A., Reilly, M.B., Xu, C., Varol, E., Oikonomou, P.,
873 Glenwinkel, L., McWhirter, R., et al. (2021). Molecular topography of an entire nervous system.
874 Cell *184*, 4329-4347.e4323. 10.1016/j.cell.2021.06.023.
875 Turek, M., Besseling, J., and Bringmann, H. (2015). Agarose Microchambers for Long-term Calcium
876 Imaging of Caenorhabditis elegans. J Vis Exp, e52742. 10.3791/52742.
877 Vowels, J.J., and Thomas, J.H. (1992). Genetic analysis of chemosensory control of dauer formation in
878 Caenorhabditis elegans. Genetics *130*, 105-123. 10.1093/genetics/130.1.105.
879 Wakabayashi, T., Kitagawa, I., and Shingai, R. (2004). Neurons regulating the duration of forward
880 locomotion in Caenorhabditis elegans. Neurosci Res *50*, 103-111. 10.1016/j.neures.2004.06.005.
881 Wang, H., Liu, J., Gharib, S., Chai, C.M., Schwarz, E.M., Pokala, N., and Sternberg, P.W. (2017).
882 cGAL, a temperature-robust GAL4–UAS system for Caenorhabditis elegans. Nature Methods
883 *14*, 145-148. 10.1038/nmeth.4109.
884 Wang, H., Park, H., Liu, J., and Sternberg, P.W. (2018). An Efficient Genome Editing Strategy To
885 Generate Putative Null Mutants in Caenorhabditis elegans Using CRISPR/Cas9. G3 (Bethesda)
886 *8*, 3607-3616. 10.1534/g3.118.200662.
887 White, J.G., Southgate, E., Thomson, J.N., and Brenner, S. (1986). The structure of the nervous system
888 of the nematode Caenorhabditis elegans. Philos Trans R Soc Lond B Biol Sci *314*, 1-340.
889 10.1098/rstb.1986.0056.
890

Figure 1

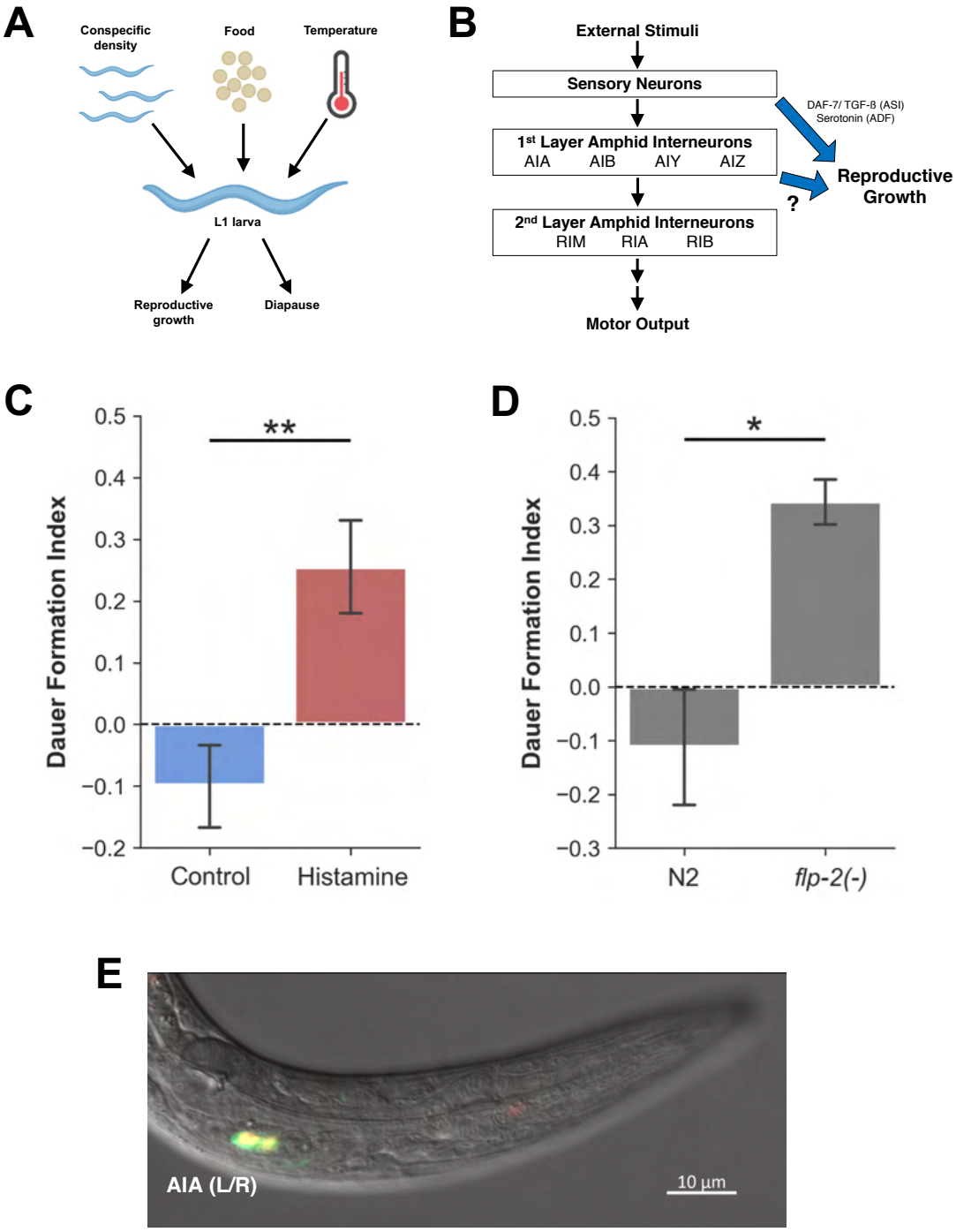
A
Conspecific density
Food
Temperature
L1 larva
Reproductive growth
Diapause
B
External Stimuli
Sensory Neurons
1st Layer Amphid Interneurons
AIA AIB AIY AIZ
2nd Layer Amphid Interneurons
RIM RIA RIB
Motor Output
DAF-7/ TGF-8 (ASI)
Serotonin (ADF)
?
Reproductive Growth
C
Dauer Formation Index
0.5
0.4
0.3
0.2
0.1
0.0
−0.1
−0.2
**
Control
Histamine
D
Dauer Formation Index
0.5
0.4
0.3
0.2
0.1
0.0
−0.1
−0.2
−0.3
*
N2
flp-2(-)
E
AIA (L/R)
10 µm

Figure 2

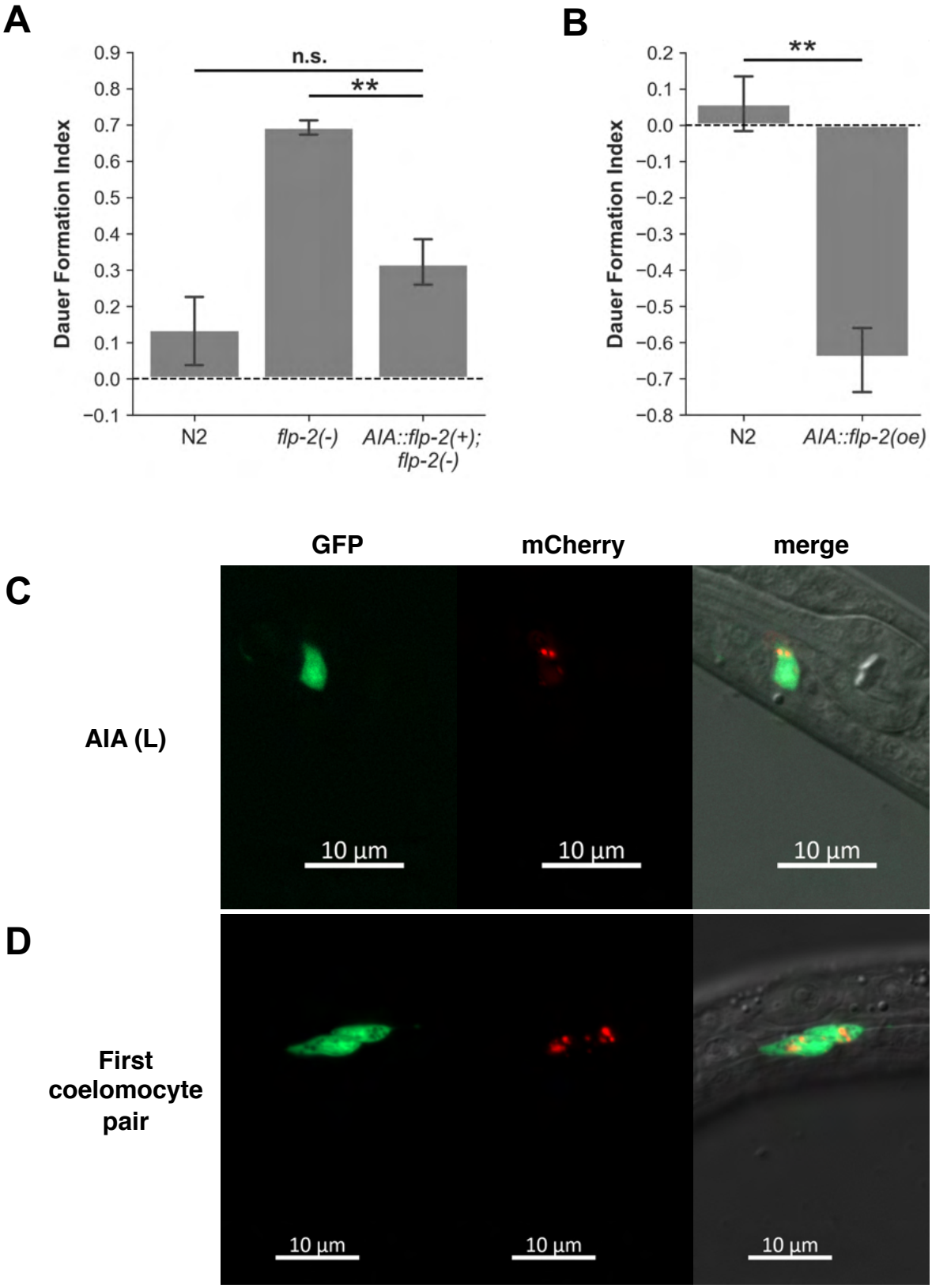
A
Dauer Formation Index
0.9
0.8
0.7
0.6
0.5
0.4
0.3
0.2
0.1
0.0
−0.1
n.s.
**
N2
flp-2(-)
AIA::flp-2(+); flp-2(-)
B
Dauer Formation Index
0.2
0.1
0.0
−0.1
−0.2
−0.3
−0.4
−0.5
−0.6
−0.7
−0.8
**
N2
AIA::flp-2(oe)
C
GFP
mCherry
merge
AIA (L)
10 µm
10 µm
10 µm
D
First coelomocyte pair
10 µm
10 µm
10 µm

Figure 3

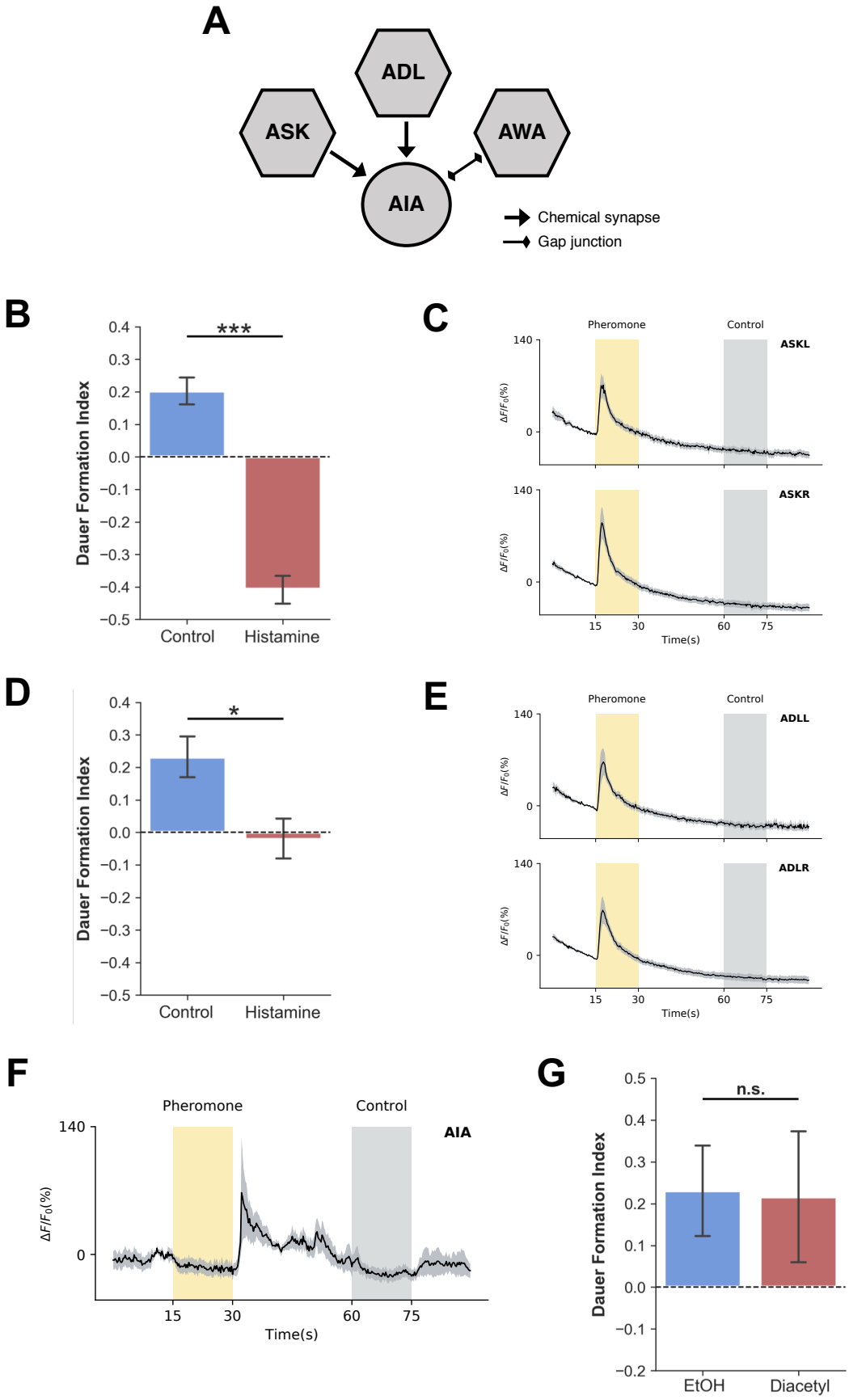
A
ADL
ASK
AWA
AIA
Chemical synapse
Gap junction
B
***
Dauer Formation Index
Control
Histamine
C
Pheromone
Control
ASKL
ASKR
ΔF/F0(%)
Time(s)
D
*
Dauer Formation Index
Control
Histamine
E
Pheromone
Control
ADLL
ADLR
ΔF/F0(%)
Time(s)
F
Pheromone
Control
AIA
ΔF/F0(%)
Time(s)
G
n.s.
Dauer Formation Index
EtOH
Diacetyl

Figure 4

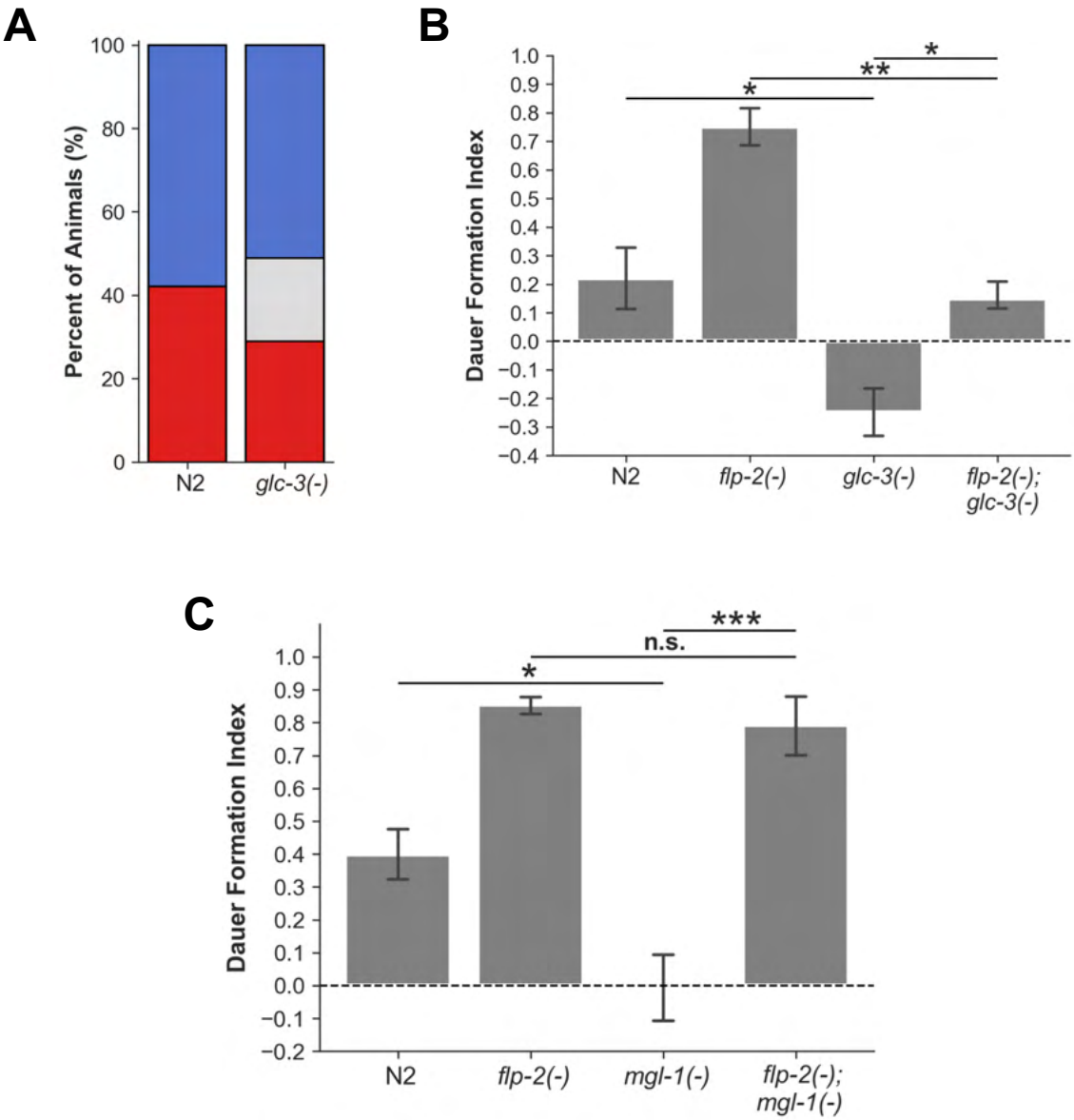
A
Percent of Animals (%)
100
80
60
40
20
0
N2
glc-3(-)
B
Dauer Formation Index
1.0
0.9
0.8
0.7
0.6
0.5
0.4
0.3
0.2
0.1
0.0
−0.1
−0.2
−0.3
−0.4
*
**
*
N2
flp-2(-)
glc-3(-)
flp-2(-);
glc-3(-)
C
Dauer Formation Index
1.0
0.9
0.8
0.7
0.6
0.5
0.4
0.3
0.2
0.1
0.0
−0.1
−0.2
***
n.s.
*
N2
flp-2(-)
mgl-1(-)
flp-2(-);
mgl-1(-)

Figure 5

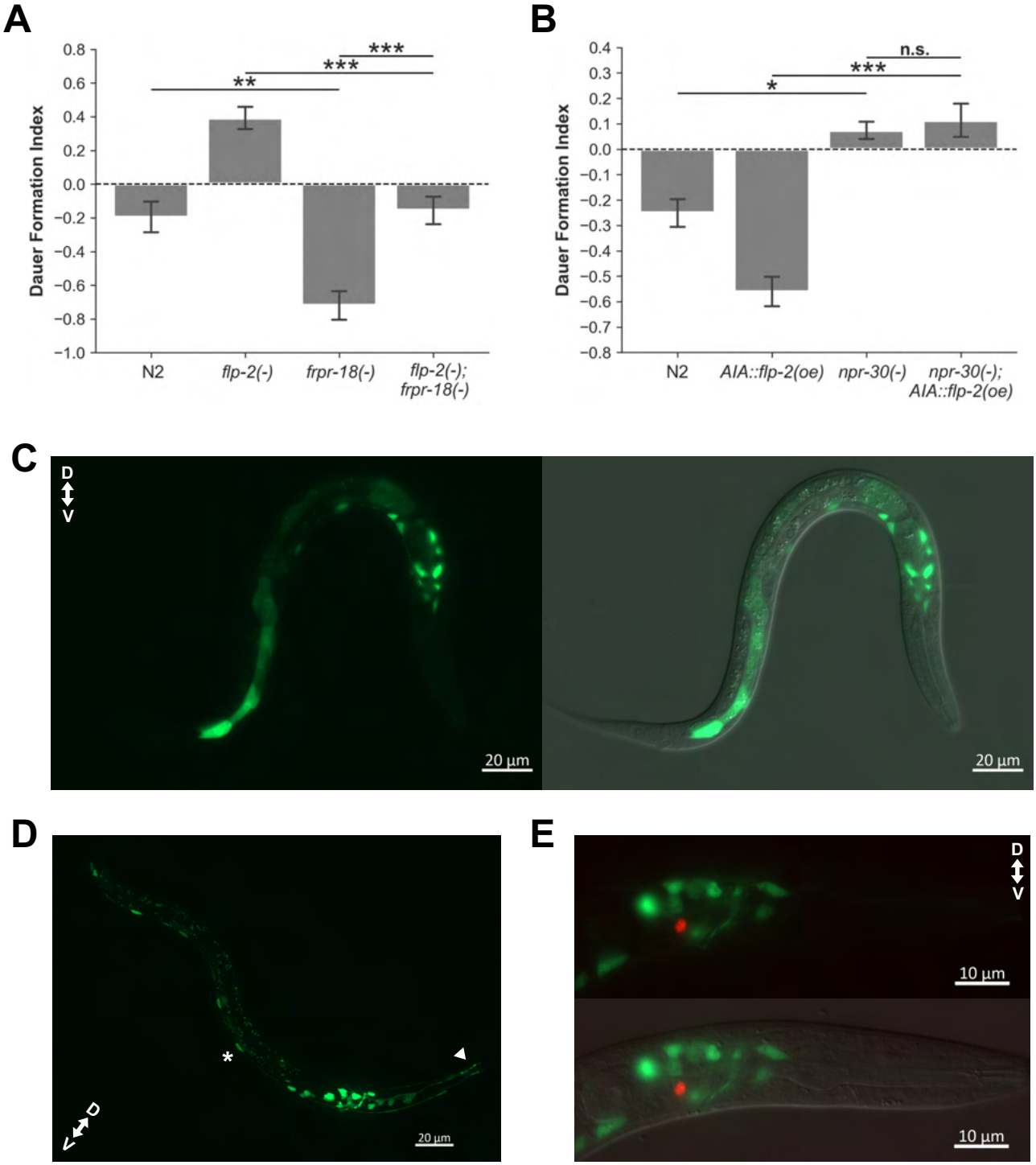
A
Dauer Formation Index
0.8
0.6
0.4
0.2
0.0
−0.2
−0.4
−0.6
−0.8
−1.0
**
***
***
N2
flp-2(-)
frpr-18(-)
flp-2(-); frpr-18(-)
B
Dauer Formation Index
0.4
0.3
0.2
0.1
0.0
−0.1
−0.2
−0.3
−0.4
−0.5
−0.6
−0.7
−0.8
*
***
n.s.
N2
AIA::flp-2(oe)
npr-30(-)
npr-30(-); AIA::flp-2(oe)
C
D
V
20 µm
20 µm
D
*
D
V
20 µm
E
D
V
10 µm
10 µm

Figure 6

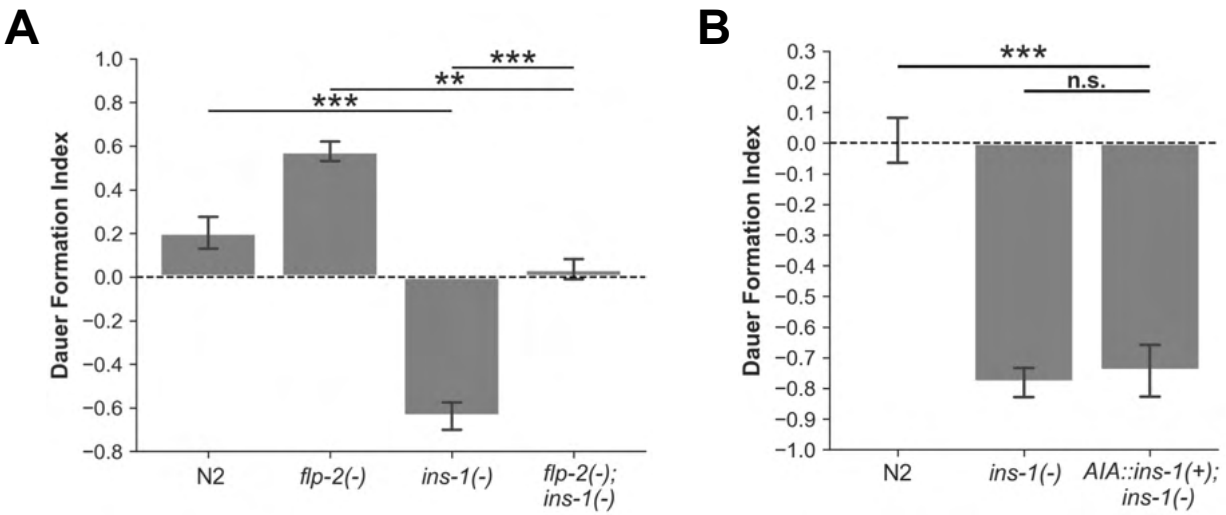

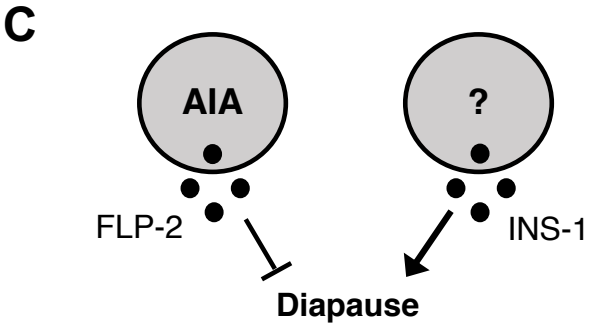

- Increased lipid storage
- Decreased fat metabolism

Figure 7

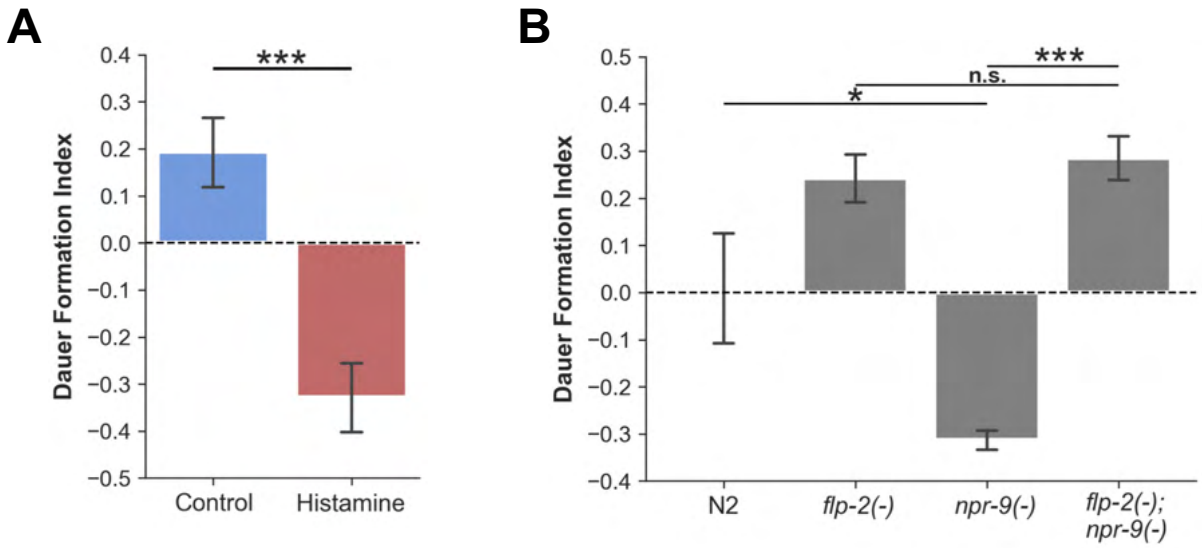
A
***
Dauer Formation Index
0.4
0.3
0.2
0.1
0.0
−0.1
−0.2
−0.3
−0.4
−0.5
Control
Histamine
B
***
n.s.
*
Dauer Formation Index
0.5
0.4
0.3
0.2
0.1
0.0
−0.1
−0.2
−0.3
−0.4
N2
flp-2(-)
npr-9(-)
flp-2(-);
npr-9(-)

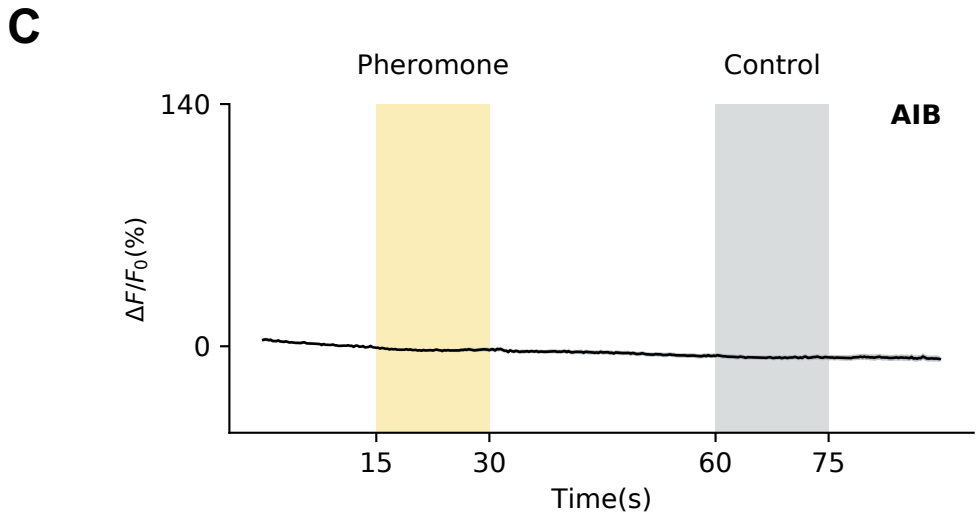
C
Pheromone
Control
AIB
140
0
ΔF/F0(%)
15
30
60
75
Time(s)

Figure 8

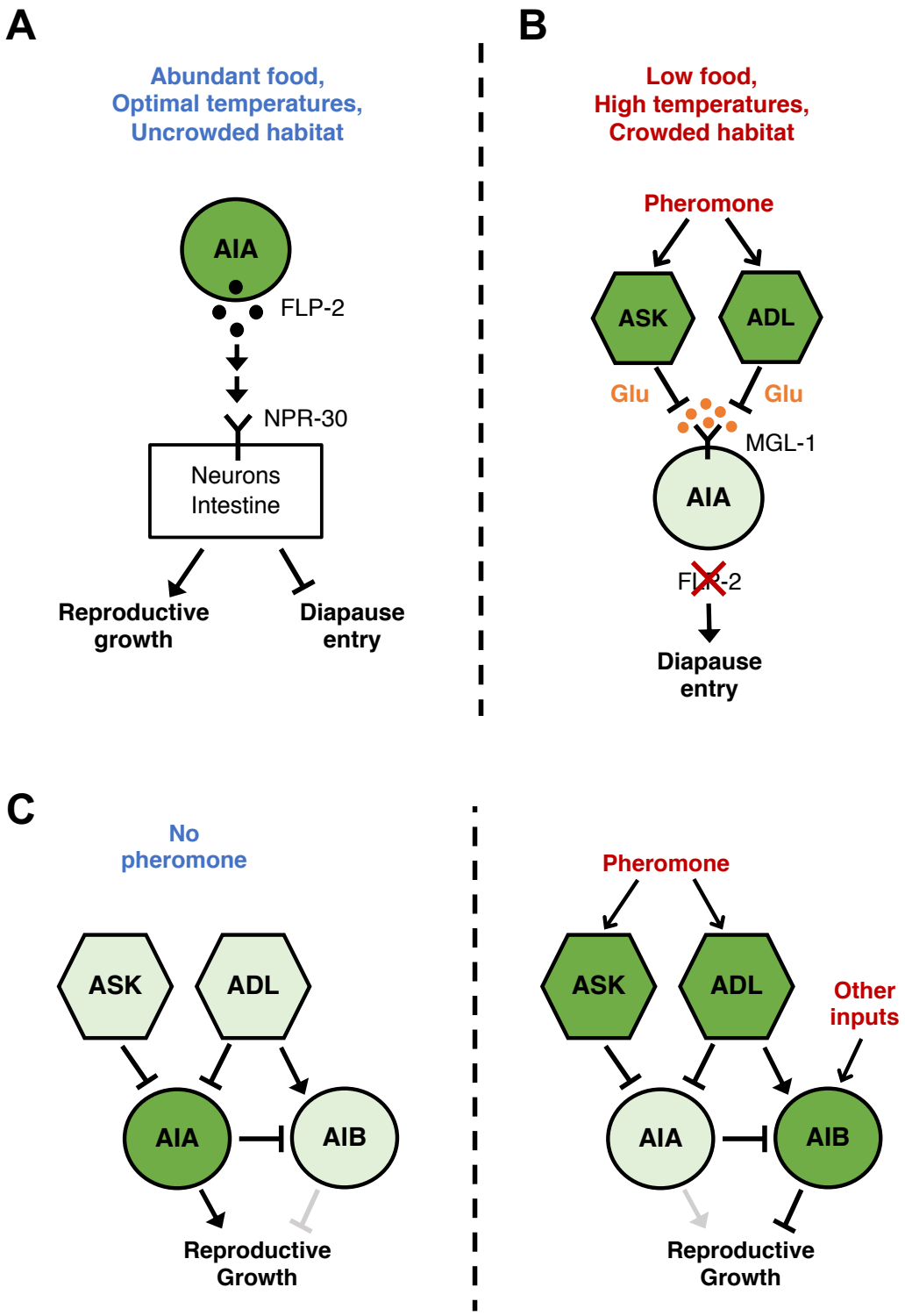
A
Abundant food,
Optimal temperatures,
Uncrowded habitat
AIA
FLP-2
NPR-30
Neurons
Intestine
Reproductive growth
Diapause entry
B
Low food,
High temperatures,
Crowded habitat
Pheromone
ASK
ADL
Glu
Glu
MGL-1
AIA
FLP-2
Diapause entry
C
No pheromone
ASK
ADL
AIA
AIB
Reproductive Growth
Pheromone
ASK
ADL
Other inputs
AIA
AIB
Reproductive Growth

Figure S1

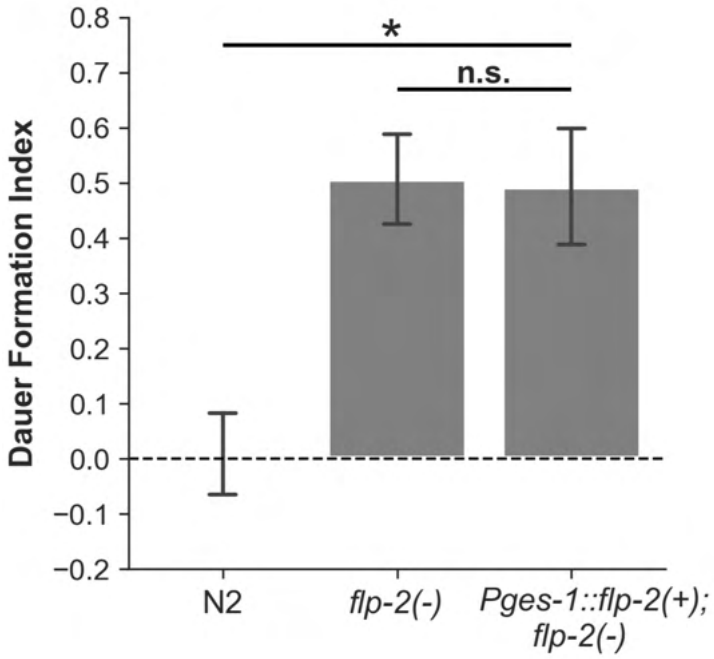
Dauer Formation Index
0.8
0.7
0.6
0.5
0.4
0.3
0.2
0.1
0.0
−0.1
−0.2
*
n.s.
N2
flp-2(-)
Pges-1::flp-2(+);
flp-2(-)

Figure S2

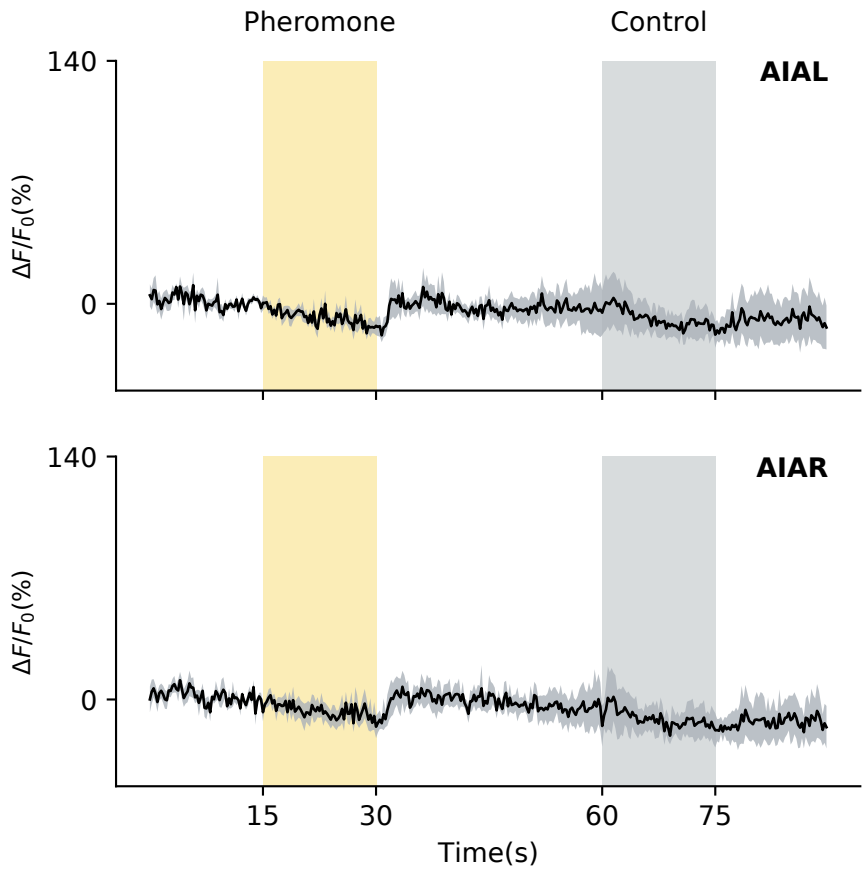
Pheromone
Control
140
0
AIAL
ΔF/F0(%)
140
0
AIAR
ΔF/F0(%)
15
30
60
75
Time(s)

Figure S3

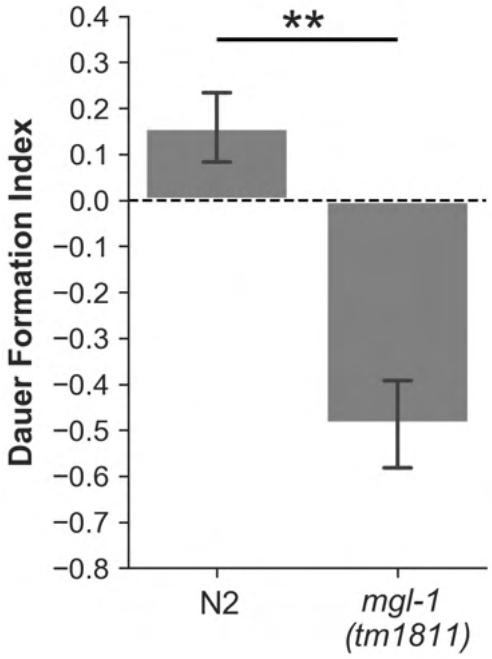
**
0.4
0.3
0.2
0.1
0.0
−0.1
−0.2
−0.3
−0.4
−0.5
−0.6
−0.7
−0.8
Dauer Formation Index
N2
mgl-1
(tm1811)

Figure S4

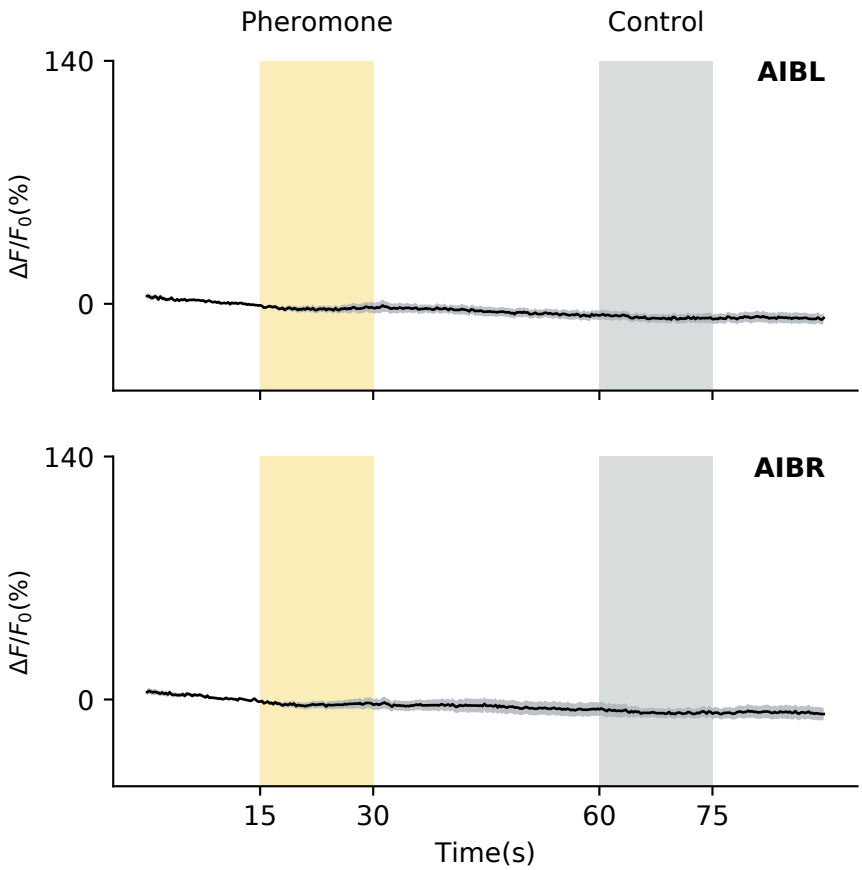
Pheromone
Control
140
0
AIBL
ΔF/F0(%)
140
0
AIBR
ΔF/F0(%)
15
30
60
75
Time(s)